Supplementary Materials

This PDF file includes:
Materials and Methods
Table S1
Figs. S1 to S14
References

Other supplementary material for this manuscript includes the following Excel files: Table S2: Mouse metabolomics.xlsx
Table S3: DEG RNA seq.xlsx (↑$[K^+]_e$ vs Ctrl)
Table S4: List of significantly enriched H3K9Ac peaks.xlsx (FDR≤0.05)
Table S5: List of significantly enriched H3K27me3 peaks.xlsx (FDR≤0.05)

Materials and methods

Study approval. Animal experiments were conducted with the approval of the NCI and NIAMS Animal Use and Care Committees and performed in accordance with NIH guidelines. All NIH cancer patients providing human samples were enrolled in clinical trials approved by the NIH Clinical Center and NCI institutional review boards. Each patient signed an informed consent form and received a patient information form before participation.

Mice and cell lines. C57BL/6 mice (obtained from Charles River Laboratories, Frederick, MD) of 6–8 weeks of age were used as recipient hosts for adoptive transfer unless otherwise indicated. pmel Ly5.1 transgenic mice were used for adoptive cell transfer and viral kinetics experiments. To obtain pmel Ly5.1mice we crossed pmel(B6.Cg-/Cy Tg [TcraTcrb] 8Rest/J) with Ly5.1 mice (B6.SJL-PtprcaPepcb/BoyJ) obtained from Jackson Laboratory. All mice were maintained under specific pathogen-free conditions. Modified B16-mhgp100 (H-2D^b), a mouse melanoma cell line, was transduced as previously described to express glycoprotein 100 (gp100) mutated to express human amino acid residues at positions 25–27 (EGS to KVP); this line was used as the tumor model. Cell lines were maintained in complete media DMEM (Gibco) with 10% FBS, 1% glutamine and 1% penicillin–streptomycin.

$[K^+]_e$ media formulation. $\uparrow[K^+]_e$ media was prepared as described previously (*22*). Unless otherwise indicated, re-activation of cells in elevated $[K^+]_e$ was performed with an isotonic RPMI formulation with an additional 40 mM of potassium for mouse cells and 50 mM for human cells in comparison to the control condition medium. Briefly, $\uparrow[K^+]_e$ medium was produced by obtaining a custom formulation of RPMI 1640 from Gibco that was devoid of NaCl. Isotonic medium containing an additional 40 mM KCl was reconstituted with a combination of NaCl and KCl such that the final inorganic salt concentrations, in mM, were: NaCl 63.4, $NaHCO_3$ 23.8, Na_2PO_4 5.6, KCl 45.3, $MgSO_4$ 0.4 and $Ca(NO_3)_2$ 0.4.

***In vitro* activation of T cells**. $CD8^+$ T cells from pmel mice were stimulated *in vitro* with 1 μM human gp100 peptide (10 μg/ml) for 5 days and secondary re-stimulation was done for 48hrs with plate-bound anti-CD3 (1μg/ml; BD Biosciences) and soluble anti-CD28 (1μg/ml; BD

Biosciences) and expanded in culture medium containing 60 IU/mL of IL-2. All conditions (e.g. Ctrl, $\uparrow[K^+]_e$, 2-HC, Acss1 over expression) were activated as listed above for a total of 10 days. For measuring T cell effector function on day 10, these cells were washed of their original culture media (experimental or control and cytokines) prior to stimulation for 5 h with anti-CD3 and anti-CD28 without IL-2 in the presence of brefeldin A and monensin (BD Biosciences).

Extracellular flux analysis. Oxygen consumption rate (OCR) and extracellular acidification rate (ECAR) were measured using a XF96 extracellular analyzer (Seahorse Bioscience) as previously described in the indicated conditions. Prior to the analysis cells were washed in PBS and subjected to live cell separation using Ficoll density separation (Lympholyte-M, CedarLane). OCR and ECAR were measured in XF medium as per manufacturing instructions (non-buffered RPMI 1640 containing 25 mM glucose, 2 mM l-glutamine, and 1 mM sodium pyruvate) under basal conditions and in response to 1 μM oligomycin, 2 μM fluoro-carbonyl cyanide phenylhydrazone (FCCP) or 100 nM rotenone with 1 μM antimycin A (Seahorse Bioscience).

Intracellular cytokine staining, phosphoflow and flow cytometry. For all flow cytometry experiments, T cells were stained with a fixable live/dead stain (Invitrogen) in PBS followed by surface antibody staining in FACS buffer (PBS with 0.5% BSA and 0.1% sodium azide). For intracellular cytokine staining, cells were first stained for surface markers and later stained for intracellular molecules following fixation and permeabilization following the manufacturer's protocols (BD Cytofix/Cytoperm). Briefly, all the cells were washed of their original culture media (experimental or control and cytokines) prior to stimulation. In the experiments depicted (**fig. S5H and fig. S7B**) cells were stimulated presence of brefeldin A and monensin in 'control' media - complete RMPI 1640 media with standard ion concentrations with FBS without IL2. For phosphoflow staining, BD PhosFlow reagents were used, and protocols were carried out according to the manufacturer's protocols. After washing, cells were stained with phospho-antibodies purchased from Cell Signaling. Antibodies for surface staining and intracellular cytokine staining were purchased from BD Biosciences, BioLegend and eBiosciences. To check BODIPY-FL C16 uptake in control or $\uparrow[K^+]_e$ treated cells, freshly prepared 1 μM BODIPY was pulsed onto T cells overnight, then washed twice with PBS prior to flow cytometry quantification or confocal microscopy. To check glucose analogue 2-NBDG (2-(N-(7-Nitrobenz-

2-oxa-1,3-diazol-4-yl)Amino)-2-Deoxyglucose) uptake, cells were pulsed with freshly prepared 10 μM NBDG for 30 min then washed twice with PBS prior to flow cytometry quantification. All experiments were conducted on a BD Fortessa flow cytometer (Becton Dickinson) and analyzed with Flow Jo software (TreeStar).

Adoptive cell transfer (ACT) and tumor immunotherapy. For immunotherapy studies, C57BL/6 mice were implanted subcutaneously with 5×10^5 cells of the melanoma line B16-mhgp100. 10 days after tumor implantation, mice (n=5-10) were sub-lethally irradiated (600 cGy), randomized, and injected intravenously with 5×10^5 pmel Ly5.1 T cells transduced with control or *Acss1* overexpression vectors or control/ $\uparrow[K^+]_e$ or control/2-HC. Post-T cell transfer mice received intraperitoneal injections of IL-2 in PBS (18×10^4 IU per 0.5 ml) once daily for 3 days starting on the day of cell transfer. T cell transfers and measurement of tumors were coded and performed in a blinded manner. Tumors were measured every two or three days after transfer and tumor area was calculated by length × width of the tumor. Mice with tumors approaching greater than 400 mm^2 were euthanized. Tumor measurement are presented as mean ± SEM at the indicated times after ACT.

Immunophenotyping, persistence and response of $CD8^+$ T cells to acute viral infection. To measure the persistence of transferred control/$\uparrow[K^+]_e$ or control/2-HC cells in tumor bearing mice, spleens from the respective groups were collected at the indicated time points for CD62L phenotyping and for quantification of absolute numbers. For experiments assessing the response of $CD8^+$ T cells to acute viral infection, 5×10^5 MSGV or *Acss1* transduced and Thy1.1-enriched pmel Ly5.1 $CD8^+$ T cells were transferred into $Thy1.2^+$ $Ly5.2^+$ recipient C57BL/6 mice. Following transfer, mice were vaccinated with 1×10^7 plaque-forming units (PFU) of recombinant human vaccinia virus expressing mhgp100. For measuring TIL phenotype, mice implanted with B16- tumors and received control/ $\uparrow[K^+]_e$ T cells were obtained on day6 or day 10. Each tumor was weighed for normalizing the absolute numbers before processing to single cell suspensions. Tumors were processed with Tissue Dissociator (gentleMACS™ Dissociator) and lymphocytes were separated from dead cells using lympholyte (Lympholyte®-M (Mouse)-Cedarlane). For measuring the persistence of TIL in Fig.4J, CD90.1 TIL were sorted from B16-tumors of the mice (n=20 per condition) receiving control/ $\uparrow[K^+]_e$ T cells. Sorted TIL are

normalized and transferred to CD 90.2 mice. Recall responses of the transferred TILs in CD90.2 host was assessed by challenging with recombinant vaccinia virus expressing gp100. Absolute numbers were enumerated on day 5 post viral challenge.

Experimental metastasis. To analyze the efficacy of adoptively transferred T cells to treat established lung tumor nodules or prevent further colonization we used B16-F10 melanoma cells recombinantly expressing mhgp100. B16-F10-gp100 (2 x10^5 cells) were intravenously injected into sub-lethally irradiated (600 cGy) mice. Ten days after implantation, mice were randomized and injected intravenously with 1 × 10^5 pmel Ly5.1 T cells treated in control (n=10) or 2-HC (n=10) conditions for 10 days. Two weeks later mice were euthanized, and lungs were collected to enumerate the lung nodules.

Retroviral transduction. Platinum-E ecotropic (PlatE) packaging cells (Cell Biolabs) were plated in complete media one day before transfections on poly-d-lysine-coated 10-cm plates (Corning) at a concentration of 6 × 10^6 cells per plate. On the day of transfection complete media was replaced with media without antibiotics. Packaging cells were transfected with 20 μg of retroviral plasmid DNA encoding MSGV-Thy1.1, MSGV-*Acss1*-Thy1.1or *Acss1*-Flag-Thy1.1, MSGV-*Acss2*-Thy1.1, MSGV-LC3-mcherry-eGFP-Thy1.1, MSGV-LC3G120A-mcherry-eGFP-Thy1.1 (G120A is an autophagy-inefficient construct) along with 12 μg pCL-Eco plasmid using 60 μL Lipofectamine 2000 in OptiMEM (Invitrogen) for 8 h. Medium was replaced 8 h after transfection and cells were incubated for a further 48 h in complete media. To capture the viral particles for efficient transduction, retroviral supernatants were spun at 2,000 x g for 2 h at 32°C in 24-well non-tissue-culture-treated plates coated with Retronectin (Takara Bio). Human peripheral blood lymphocytes (PBL) were transduced with the NY-ESO-1 TCR following similar procedures as described above with 293GP cells as packaging cells and RD114 helper plasmid.

Confocal and live cell imaging. Live cell imaging was performed on LC3-mcherry-eGFP-Thy1.1 or G120A transduced T cells to monitor the autophagy flux. 10,000 cells were seeded in an 8 well chamber slide and at least 10 images were taken for each condition. To observe the co-localization of ACSS1 in the mitochondria, *Acss1*-FlagThy1.1$^+$ T cells were used. MitoTracker

Green was used to stain mitochondria and Cy3-conjugated anti-Flag was used for *Acss1*-Flag. MSGV-Thy1.1 cells were used as negative control for background against Cy3-conjugated anti-Flag. A Nikon Ti2-E microscope (Nikon Instruments, Inc., Melville, NY) equipped with a CSU-W1 spinning disk unit (Yokogawa Corp. of America, Newnan, GA), Hamamatsu ORCA Flash 4 v3.0 sCMOS camera (Hamamatsu Photonics K.K, Bridgewater, NJ), motorized stage, and 60x plan-apochromat (N.A.1.4) objective lens was used to acquire images of Biodipy-FL C16 labelled cells. The same imaging parameters were used for all images in the dataset. Images were collected using the accompanying Nikon Elements software (v4.2) with same linear lookup-table (LUT) applied to all images in the dataset before being exported as Tiff files. The exported files were arranged and composed into figures using Adobe Photoshop.

Metabolomics. For intracellular metabolite measurements in T cells exposed to Ctrl / ↑$[K^+]e$, $4*10^6$ cells were collected in Eppendorf tubes and briefly washed twice with 1 mL ice cold PBS before snap freezing in liquid nitrogen. 1 mL 80% methanol/water (pre-cooled in −80°C freezer) was added to frozen pellets to extract the metabolites. Samples were centrifuged at 20000g for 10 min at 4°C, and the supernatant was concentrated using a speed vacuum concentrator. In brief, Metabolomic analyses were performed as described using LC Q Exactive Plus Mass Spectrometer (LC-QE-MS) (Thermo Scientific) (*44*). Metaboanalyst was used to range-scale data and provide pathway analysis of metabolites significantly changed (1.5-fold difference, $P<0.05$)(www.metaboanalyst.ca/).

AcCoA and Citrate quantification. T cells (n=3) cultured in control or ↑$[K^+]_e$ or 2-HC conditions were collected and washed in PBS to perform analysis of total and cytoplasmic AcCoA and citrate levels. For extraction of cytoplasmic AcCoA and citrate, samples were homogenized in 1% Triton X-100, 20 mM Tris-HCl, pH=7.4, 150 mM NaCl on ice for 10 min. Samples were then centrifuged at 20000 g for 10 min at 4C to pellet nuclei and mitochondria. Supernatant obtained after centrifugation was used as the nucleocytosolic fraction to measure AcCoA or citrate by fluorometric assay (Ex=535, Em=587) or by HPLC. The following kits were used (Acetyl-Coenzyme A Assay Kit –MAK039; Sigma); (Citrate Assay Kit- MAK057; Sigma) to quantify citrate and AcCoA. For total cellular AcCoA quantification, pelleted cells were extracted using 80% methanol or 5% sulfo-salicylic acid with 50µM DTT. Briefly, cells

were frozen in liquid nitrogen and thawed on ice 2 two times before deproteinizing with a 10 kDa MWCO spin filter prior to the assay. AcCoA concentrations were interpolated with AcCoA standards using fluorometric assay (Ex=535, Em=587) or by mass spectrometry. Citrate concentrations were interpolated with citrate standards using colorimetric assay (570 nm).

For measuring AcCoA using HPLC, samples were transferred into SUN-SRi Glass Microsampling Vials (Thermo Fisher) and 40 µl of each sample was separated using an Agilent 1100 HPLC (Agilent Technologies) equipped with a reverse phase column, Luna 3 µm C18(2) 100 Å, 150 x 4.6mm (Phenomenex). The HPLC-reverse phase column was calibrated with variable concentrations (2, 4, 8, 16, and 32ug/mL) of acetyl-CoA (Sigma). The mobile phase was described by Shibata et al., and consisted of two eluents: 75 mM sodium acetate, 100 mM NaH_2PO_4 pH 4.6 (buffer A). Methanol was added to the buffer A at a ratio of 70:30 (v/v) = buffer A:methanol (buffer B). The gradient was starting with 10% of buffer B, 10min at up to 40% of buffer B, 13min at up to 68% of buffer B, 23min at up to 72% of buffer B, 28min at up to 100% of buffer B, and hold for additional 5min. The initial condition was restored after 10min with 10% of buffer B. The flow rate was 0.6ml/min and the detection were performed at 259 nm. UV chromatograms were analyzed using a software, ChemStation version B. 04.03 (Agilent Technologies)(*45*).

Electron Microscopy. T cell pellets (n=3) cultured in control or $\uparrow[K^+]_e$ were fixed in 2% glutaraldehyde and 0.1 M Sodium cacodylate buffer. These cells were further processed for Transmission Electron Microscopy (TEM); with two washes of 0.1 M Sodium cacodylate buffer for 10 min each and then post fixation with 1% Osmium tetroxide in 0.1 M and 0.1 M Sodium cacodylate buffer for an hour at room temperature. Then the cells were washed twice with 0.1 M Sodium cacodylate buffer for 10 min, and one wash of 0.1M Sodium acetate buffer for 10 min. Later, cells were stained with 0.5% Uranylacetate (UA) in 0.1M Sodium acetate buffer for one hour at RT. After staining with UA, cells were washed twice with 0.1M Sodium acetate buffer for 10 min. Pellets went through dehydration in a graded ethanol series (50%, 70%, 90%, 95%, 100%). Cells were cross linked with Propylene oxide and then infiltrated in 100% polyscience resin for overnight at RT. On the following day, resin was changed twice and incubated at 55C oven for 48 hours. When the resin is cured, blocks were ultra-thin sectioned (70-80nm) and

stained for 1:1 0.5% UA in ddH_2O and 70% ethanol for two minutes and rinsed with ddH_2O, then stained with 1:1 Leadcitrate and ddH_20 and later rinsed with ddH_2O. After blotting the grids were carbon coated with TedPella Evaporator and imaged with Hitachi 7600.

RNA sequencing and analysis. RNA-Seq analysis was performed on *in vitro* cultured day 10 $CD8^+$ T cells from $\uparrow[K^+]_e$ and control with 3 culture replicates. RNA-Seq was performed as described previously. Briefly, a total of 200ng of total RNA was used to prepare the RNA-Seq library by using TruSeq RNA sample prep kit (FC-122-1001, Illumina). Approximately 40 million reads were sequenced and aligned to mouse genome (NCBI37/mm9) with TopHat 2.0.11(*46*). Only uniquely retained mapped reads were used to calculate differentially expressed genes using egdeR or Cuffdiff software packages (*47*, *48*). Fisher's exact test or t-test were used to evaluate significance with indicated P value and fold-change thresholds.

ChIP-sequencing and ChIP-PCR. Chromatin Immunoprecipitations were performed with validated antibodies from previous literature (*39*, *40*) and protocols were followed according to manufacturing instructions provided by the ChIP-IT Express Shearing Kit (Active Motif). Briefly, $CD8^+$ pmel cells cultured in control or $\uparrow[K^+]_e$ were fixed with formaldehyde for 7 minutes on a rocking platform and quenched with 1X of Glycine. Cells were pelleted with PMSF and protein inhibition cocktail and stored at -80ºC prior to cell lysis. Thawed cells were suspended in ice cold lysis buffer to obtain nuclei material. Nuclei material was sheared by incubating with enzymatic cocktail for 15 minutes at 37ºC. Sheared chromatin with a total of 15ug/sample was spiked with 50 ng of spike in DNA(Active motif Cat# 53083) and incubated with protein G magnetic beads with anti-H3K27Ac (Abcam Cat# ab4729), H3K9Ac (Abcam Cat# ab4441) , H3K27me3 (Abcam Cat #ab19547)7 spike in antibody (Active motif Cat# 61686) and anti IgG at 4ºC overnight. Magnetic beads were washed with buffers to remove unbound immune complexes and eluted with 150ul of elution buffer. Obtained DNA was reverse crosslinked and purified by phenol chloroform extraction. Concentration of the ChIP DNA was measured using a highly sensitive DNA assay protocol on TapeStation (Agilent) to normalize the DNA. Samples were sequenced on an Illumina NextSeq with 75bp reads in single end mode with approximately 40M reads per sample. To validate the ChIP-Seq results, we performed ChIP-PCR on the *Cd3e* and *Ifng* loci and normalized the enrichment to spike in chromatin (Active motif -

guidelines for qPCR normalization). ChIP enrichment and efficiency in different treatment conditions at the *Ifng* or *Cd3e* loci were performed by qPCR using the SYBR Green PCR master mix (ABI). Chromatin enrichment for different treatment conditions was extrapolated with the standard curve produced from diluting the input DNA. The following primers were used for qPCR: *Cd3e* promoter-F: 5'- TCAGTGTG GAGGTGCTTTG-3', *Cd3e* promoter-R: 5'-CAGCCTTCCCATAAGGATGAA-3'; *Ifng* promoter-F:5'-GGAGCCTTCGATCAGGTATAAA-3' *Ifng* promoter-R: 5' -CTCAAGTCAGAGGGTCCAAAG-3'; *Pdcd1*_Enhancer-F: 5'-GTGACTTGGCTCAAGGATGT-3', *Pdcd1*_Enhancer-R: 5'- TTG ATGGGTCCTGCGTAAAG. *Pdcd1*_TSS-F: 5'-TACAGGGTAGTGAGGAGTAAGG-3' *Pdcd1*_TSS-R: 5'-GTTCATATCCCTGGCCTCATAG-3'

ChIP-Seq and peak calling analysis. Sequenced reads with single end 75 bp were obtained by using the Illumina Pipeline. Sequenced reads were trimmed for adapters and aligned to the mouse genome (NCBI37/mm9) with Bowtie v2 and only uniquely mapped reads were retained. The output of Bowtie was converted to BAM files, which represent the genomic coordinates of each read. Bam files were normalized using RPKM and converted to coverage tracks in big wig format using Deeptools (Command #BamCoverage -b Bam_File --normalizeUsingRPKM --binSize 10 --smoothLength 30 -bl mm9.blacklist.bed --centerReads --minMappingQuality 30 -o Output_File.bw). Tracks generated were viewed using the IGV (Integrative Genomics Viewer). Peaks were called using Homer software with (# findPeaks Tag_directory -i Input -region -size 1000 -minDist 2500 >Output.txt) and the statistical significance for enrichment between control and $[K^+]_e$ conditions was calculated on 2 biological replicates with Deseq2. Volcano plots were plotted with Log fold change, which are calculated from normalized read counts of the peaks annotated to nearest TSS (homer.ucsd.edu/ getDiffExpression.pl) versus P-values obtained from Desq2 output files. Effector and Exhausted gene list Table. S7 (*37*) was used to interrogate the H3K9Ac deposition for **Fig.3I and fig.S5B**. Source of effector gene list for **Fig.3H**: differentially expressed mRNA transcripts in effector subset ($CD44^+CD62L^-$) compared to naïve ($CD44^-CD62L^+$) $CD8^+$ T cells were used to interrogate the H3K9Ac deposition in the indicated conditions. In brief, naïve $1e^6$ ($CD44^-CD62L^+$) OT-I TCR-Tg $Rag^{-/-}$ $Ly5.2^+$ $CD8^+$ splenocytes were transferred into to $Ly5.1^+$ hosts followed by $4e^7$ PFU of recombinant human vaccinia virus

expressing ovalbumin antigen to obtain the T cell effector subset ($CD44^{+}CD62L^{-}$) 5 days post-infection.

CRISPR-Cas9 mediated ATG7 deletion. Non-targeting control sgRNA and autophagy related 7 (ATG7) modified single guide RNAs (sgRNAs) were purchased and synthesized by Synthego. Mixture of synthetic sgRNA + Cas9 nuclease $+1*10^6$ activated T cells were suspended in 100ul of electroporation buffer (Neon transfection, Thermo Fisher) and later electroporated using Neon transfection (Thermo Fisher, setting: 1600V, 10 milliseconds, 4 pulses). T cells were re-stimulated on day 6 for 48 hrs. with CD3CD28 (1 μg/mL) and later cultured without CD3, CD28 for another 3 days with a total of cells cultured for 10 days in control or $\uparrow[K^+]_e$ ($\uparrow[K^+]_e$ = additional 40 mM).

Immunoblot analysis. Western blot analysis was performed using standard protocols. Proteins were separated by 4%–12% SDS-PAGE, followed by standard immunoblot analysis using anti–Acss1(Abcam-ab224176), Acss2 (Abcam- ab66038), LC3A/B (D3U4C; Cell Signaling), Acetylated-Lysine (Ac-K-103; Cell Signaling), p-AMPK(2531S), and β-actin (Cell Signaling). In brief, for immunoblot quantifications, cells were resuspended in total cell extraction buffer and kept on ice for 10 min followed by homogenization. Cells were then centrifuged at 20,000g for 20 min at 4°C to pellet cell debris. Detection of proteins was performed using secondary antibodies conjugated to horseradish peroxidase-HRP and the super signal west pico chemiluminescent substrate (Thermo Scientific-Pierce).

Statistical analysis. For adoptive transfer experiments, recipient mice were randomized before cell transfer. Tumor measurements were plotted as the mean ± SEM for each data point, and tumor treatment graphs were compared by using the Wilcoxon rank sum test and analysis of animal survival was assessed using a log-rank test. In all cases, two tailed test with P values of less than 0.05 were considered significant. Statistics were calculated using GraphPad Prism 7 software (GraphPad Software Inc.).

Table S1

Pt ID	Somatic mutation generated neo-antigen	Histology
A	TRIP12	Melanoma
B	SRPX	Melanoma
C	HYAL2	Lung
D	HISTHIC	Ovarian
E	HISTIH3B	Colon
F		Melanoma
G		Melanoma

Fig. S1

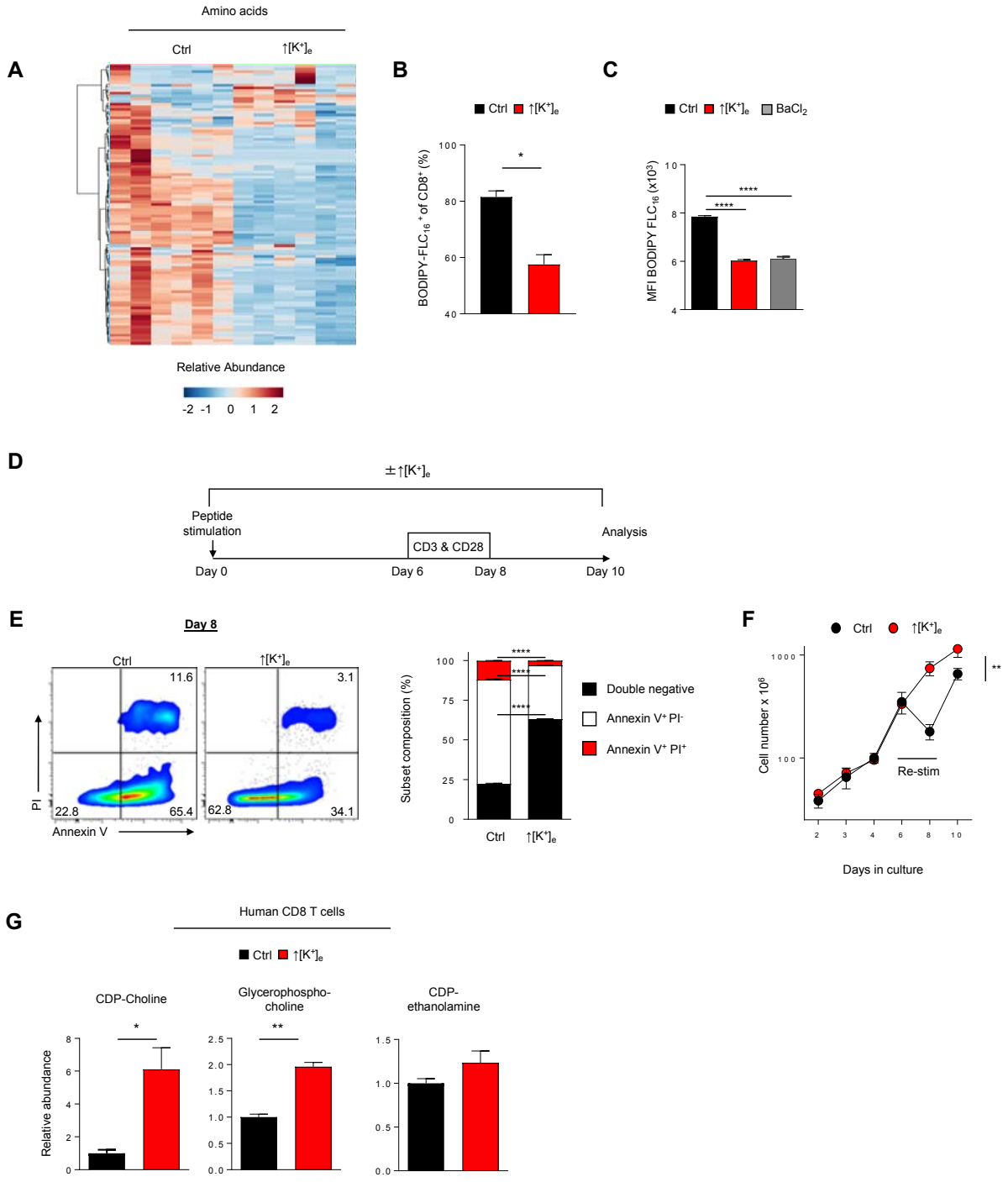
A
Amino acids
Ctrl
↑[K+]e
Relative Abundance
-2 -1 0 1 2
B
Ctrl ↑[K+]e
BODIPY-FLC16+ of CD8+ (%)
C
Ctrl ↑[K+]e BaCl2
MFI BODIPY FLC16 (x10³)
D
±↑[K+]e
Peptide stimulation
CD3 & CD28
Analysis
Day 0
Day 6
Day 8
Day 10
E
Day 8
Ctrl
↑[K+]e
11.6
3.1
22.8
65.4
62.8
34.1
PI
Annexin V
Subset composition (%)
Double negative
Annexin V+ PI-
Annexin V+ PI+
F
Ctrl ↑[K+]e
Cell number x 10⁶
Re-stim
Days in culture
G
Human CD8 T cells
Ctrl ↑[K+]e
CDP-Choline
Glycerophospho-choline
CDP-ethanolamine
Relative abundance

fig. S1. Dysregulated extracellular ↑$[K^+]_e$ ion gradients limit nutrient processing and alter cellular metabolism

(A) Heat map depicting abundance of amino acids in murine pmel T cells under control and↑$[K^+]_e$ conditions. (**B**) Statistics of **Fig. 1E** showing quantification of cells with Bodipy FLC_{16} uptake in the indicated conditions. (**C**) Quantification showing reduced Bodipy FLC_{16} uptake in the presence of non-selective potassium channel inhibitor $BaCl_2$(2 mM). Values indicate average geometric MFI, data show mean +/- SEM and is representative of two independent experiments. (**D**) Experimental set-up for *in vitro* culture conditions of pmel $CD8^+$ T cells with gp100 (10μg/ml) peptide in the presence of splenocytes for 5 days, followed by 48 hrs of re-stimulation with αCD3/αCD28 (1 μg/mL plate bound). Cells were later cultured without stimulating antibodies for an additional 3 days for a total of 10 day culture in control or ↑$[K^+]_e$ (↑$[K^+]$e= additional 40 mM). (**E, F**) Representative FACS plots defining the percentages of live (Annexin V $^-PI^-$), early apoptotic (Annexin V^+PI^-) and late apoptotic and necrotic populations (Annexin V^+ $PI^{+)}$ cultured in indicated conditions and enumeration of absolute $CD8^+$ T cell numbers over the course of culture. (**G**) Subset of enriched Kennedy pathway intermediates involving in autophagy flux in human $CD8^+$ T cells. For all relevant figures, data show mean +/- SEM and is representative of at least two independent experiments with n = at least three culture replicates, two-tailed t-tests, asterisks indicating significance are * $P < 0.05$; ** $P < 0.01$; *** $P < 0.001$; **** $P < 0.0001$ between selected relevant comparisons

Fig. S2

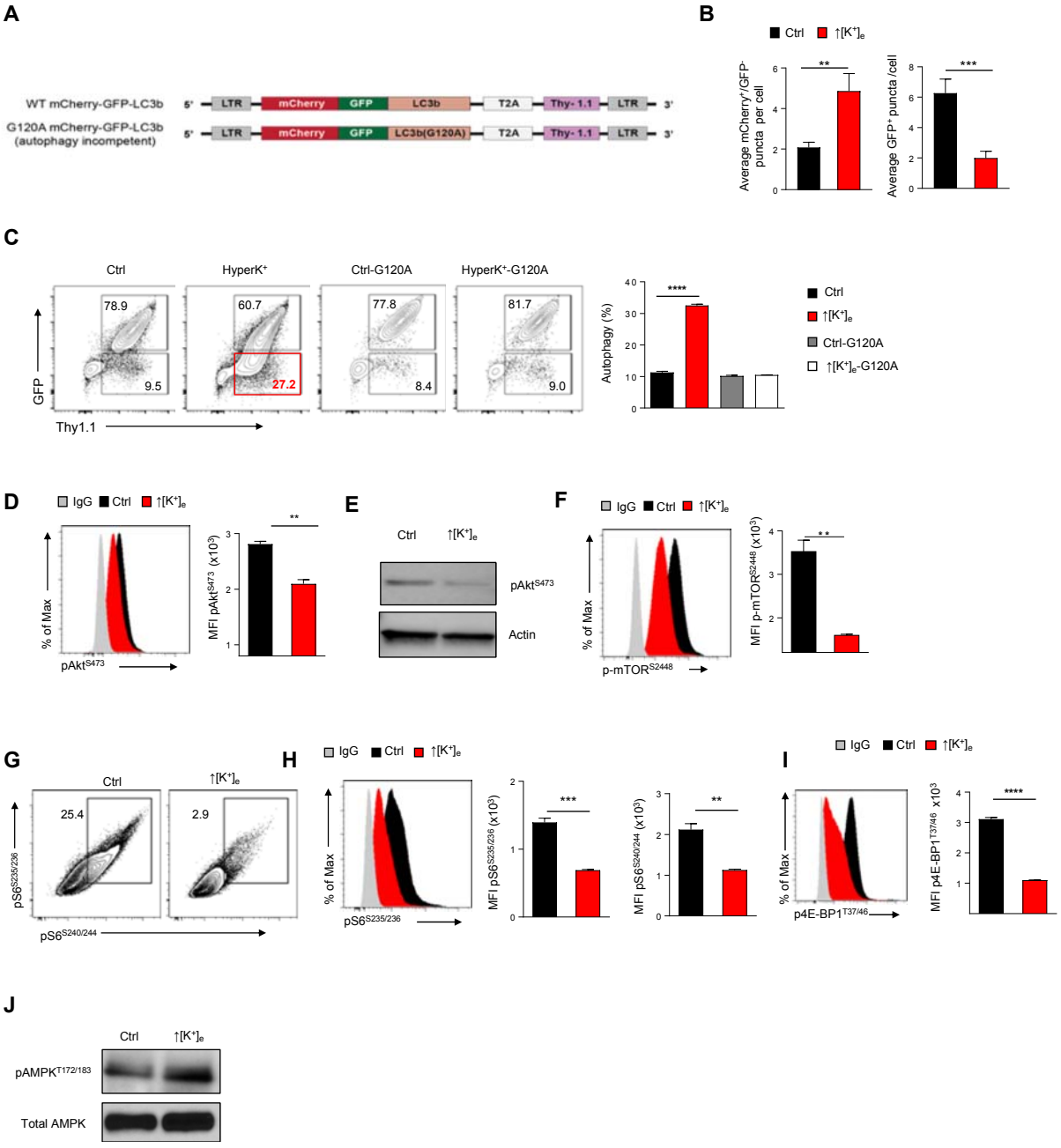
A
WT mCherry-GFP-LC3b
G120A mCherry-GFP-LC3b (autophagy incompetent)
5'
LTR
mCherry
GFP
LC3b
LC3b(G120A)
T2A
Thy-1.1
LTR
3'
B
Ctrl
↑[K+]e
Average mCherry+/GFP- puncta per cell
Average GFP+ puncta /cell
C
Ctrl
HyperK+
Ctrl-G120A
HyperK+-G120A
78.9
9.5
60.7
27.2
77.8
8.4
81.7
9.0
GFP
Thy1.1
Autophagy (%)
Ctrl
↑[K+]e
Ctrl-G120A
↑[K+]e-G120A
D
IgG
Ctrl
↑[K+]e
% of Max
pAktS473
MFI pAktS473 (x10³)
E
Ctrl
↑[K+]e
pAktS473
Actin
F
IgG
Ctrl
↑[K+]e
% of Max
p-mTORS2448
MFI p-mTORS2448 (x10³)
G
Ctrl
↑[K+]e
25.4
2.9
pS6S235/236
pS6S240/244
H
IgG
Ctrl
↑[K+]e
% of Max
pS6S235/236
MFI pS6S235/236 (x10³)
MFI pS6S240/244 (x10³)
I
IgG
Ctrl
↑[K+]e
% of Max
p4E-BP1T37/46
MFI p4E-BP1T37/46 x10³
J
Ctrl
↑[K+]e
pAMPKT172/183
Total AMPK

fig. S2. ↑$[K^+]_e$ triggers a functional program of autophagy and nutrient renewal
(A) Illustration of the MSGV retroviral constructs encoding the autophagy gene microtubule associated protein light chain 3 beta (LC3b) in conjunction with mCherry, GFP and Thy1.1 marker. Replacement of the LC3b glycine at amino acid 120 position with alanine is used as an autophagy incompetent construct. **(B)** Quantification of GFP and mCherry puncta of live cell confocal images represented in **Fig. 2B** treated under indicated conditions. **(C)** Representative flow cytometry plots and quantification of autophagy flux by measuring the loss of GFP signal within the transduced ($Thy1.1^+$) populations. **(D, E**) Representative immunoblot, flow cytometry and quantification of phospho-AKT (S473) in indicated conditions. (**F, G, H, I**) Representative flow cytometry and quantification phosphorylation of p-mTOR (S2448) and mTOR signaling downstream targets ribosomal protein S6 (S240/244) (S235/236) kinases and phospho-4EBP1 (T37/46), stimulated under anti-CD3 and anti-CD28 cross-linking in the indicated conditions (**J**) Immunoblot showing increased phosphorylation of the AMP-activated protein kinase (AMPK) in ↑$[K^+]_e$ compared to Ctrl cells. For all relevant figures, data show mean +/- SEM and is representative of at least two independent experiments with n = at least three culture replicates, two-tailed t-tests, asterisks indicating significance are * $P < 0.05$; ** $P < 0.01$; *** $P < 0.001$; **** $P < 0.0001$ between selected relevant comparisons.

Fig. S3

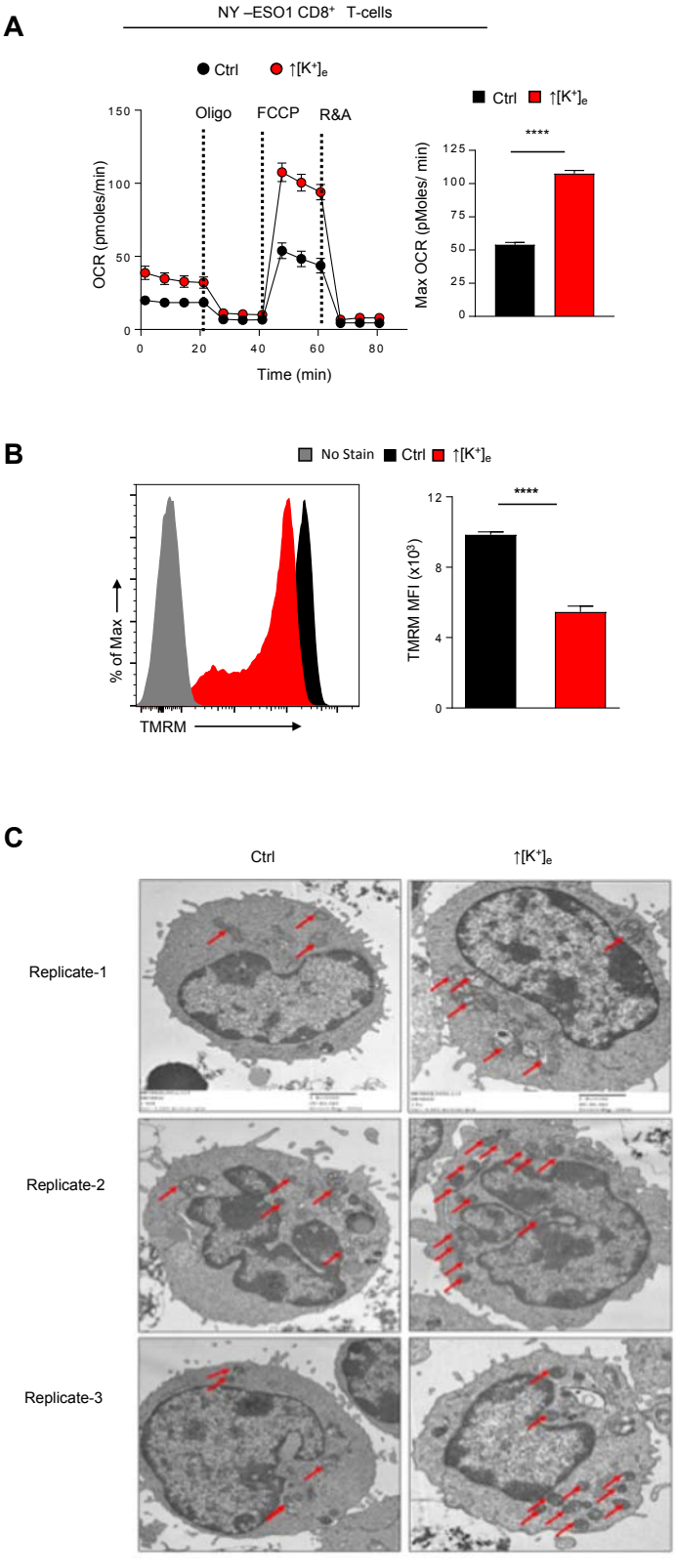
A
NY –ESO1 CD8⁺ T-cells
Ctrl
↑[K⁺]e
Oligo
FCCP
R&A
OCR (pmoles/min)
Time (min)
Max OCR (pMoles/ min)
****
B
No Stain
% of Max
TMRM
TMRM MFI (x10³)
****
C
Ctrl
↑[K⁺]e
Replicate-1
Replicate-2
Replicate-3

fig S3. Culturing $CD8^+$ T cells in $\uparrow[K^+]_e$ preserves oxygen consumption capacity and mitochondrial integrity

(A) Representative O_2 consumption rates (OCR) of $CD8^+$ T cells genetically engineered with NY –ESO-1 obtained from PBL of a melanoma patient and cultured in control or $\uparrow[K^+]_e$. (**B**) Representative FACS histograms and quantification showing low mitochondrial membrane potential ($\Delta\psi$) of human $CD8^+$ T cells cultured in $\uparrow[K^+]_e$. Values indicate average geometric MFI, data show mean +/- SEM and is representative of two independent experiments, two-tailed t-tests, asterisks indicating significance are * $P < 0.05$; ** $P < 0.01$; *** $P < 0.001$; **** $P < 0.0001$ between selected relevant comparisons.(**C**) Representative scanning electron micrographs of $CD8^+$ T cells cultured in control (n=3) or $\uparrow[K^+]_e$ (n=3). Electron micrographs showing 85% of the cells are degenerative cells with severe mitochondrial structural damage in control compared to $\uparrow[K^+]_e$. Red arrows indicate the abundance of mitochondria in indicated conditions.

Fig. S4

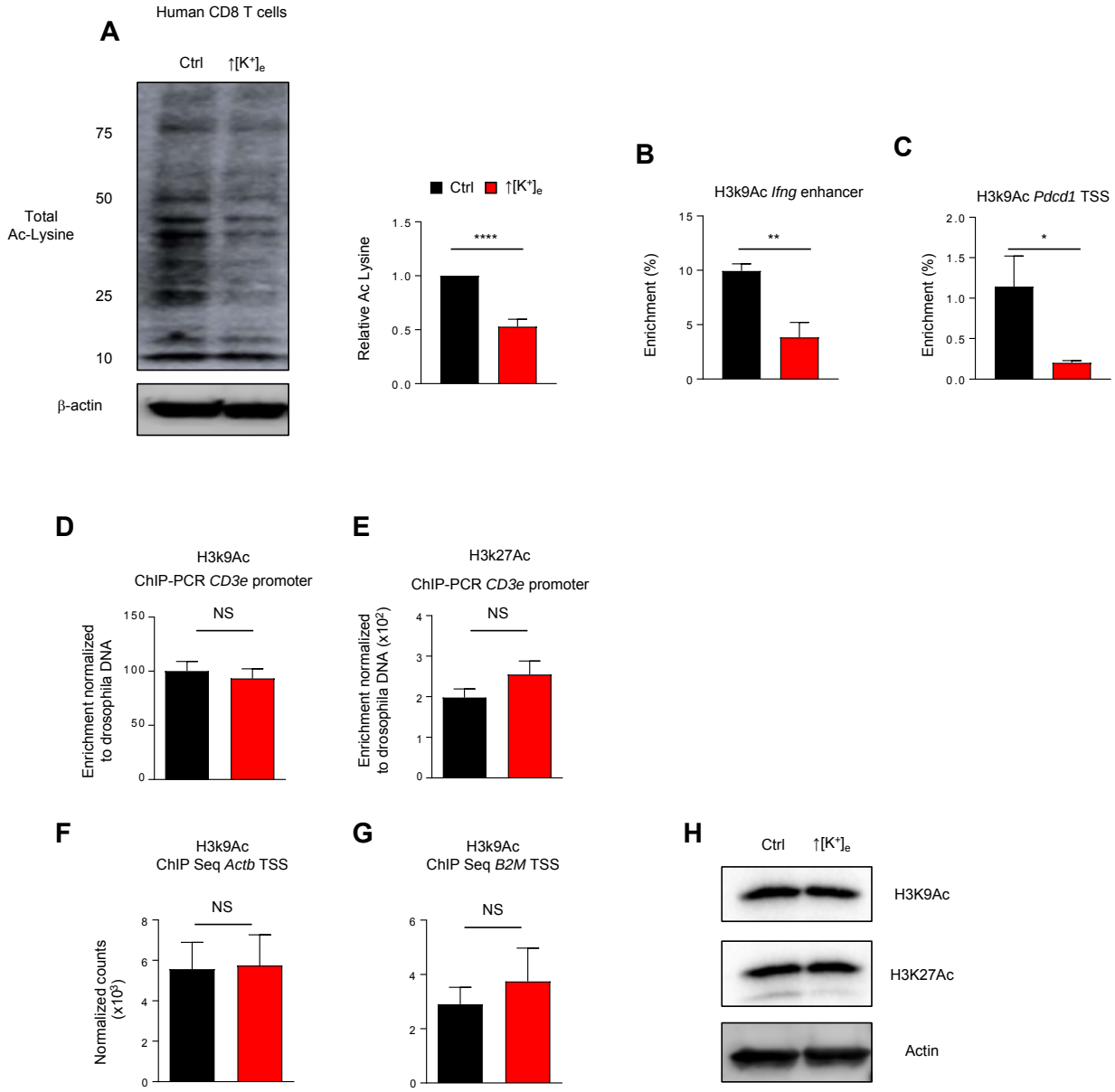
A
Human CD8 T cells
Ctrl
↑[K+]e
75
50
25
10
Total
Ac-Lysine
β-actin
Ctrl
↑[K+]e
Relative Ac Lysine
****
B
H3k9Ac Ifng enhancer
Enrichment (%)
**
C
H3k9Ac Pdcd1 TSS
Enrichment (%)
*
D
H3k9Ac
ChIP-PCR CD3e promoter
Enrichment normalized to drosophila DNA
NS
E
H3k27Ac
ChIP-PCR CD3e promoter
Enrichment normalized to drosophila DNA (x10²)
NS
F
H3k9Ac
ChIP Seq Actb TSS
Normalized counts (x10³)
NS
G
H3k9Ac
ChIP Seq B2M TSS
NS
H
Ctrl
↑[K+]e
H3K9Ac
H3K27Ac
Actin

fig. S4 ↑$[K^+]_e$ mediated metabolic programming depletes cytoplasmic AcCoA to preserve epigenetic stemness

(A) Representative immunoblot of human $CD8^+$ T cells showing reduced protein acetylation on lysine residues and quantification (right) in the indicated conditions. Data show mean +/- SEM of two independent experiments.(**B, C**) Quantifications of enrichment by ChIP-PCR at the *Ifng* enhancer and *Pdcd1* transcription start site locus. **(D, E)** Quantifications showing no significant differences in H3K9Ac and H3K27Ac deposition at the *Cd3e* loci by ChIP-PCR. **(F, G)** Quantification of the normalized read counts of the peaks associated with non-effector genes *Actb* and B*2m*. (**H**) Representative acetylation immunoblots showing total histone lysine 9 (H3K9ac) and lysine 27 (H3K27ac) in indicated conditions. For all relevant figures, data show mean +/- SEM and is representative of at least two independent experiments with n = at least three culture replicates, two-tailed t-tests, asterisks indicating significance are * $P < 0.05$; ** $P < 0.01$; *** $P < 0.001$; **** $P < 0.0001$ between selected relevant comparisons.

Fig. S5

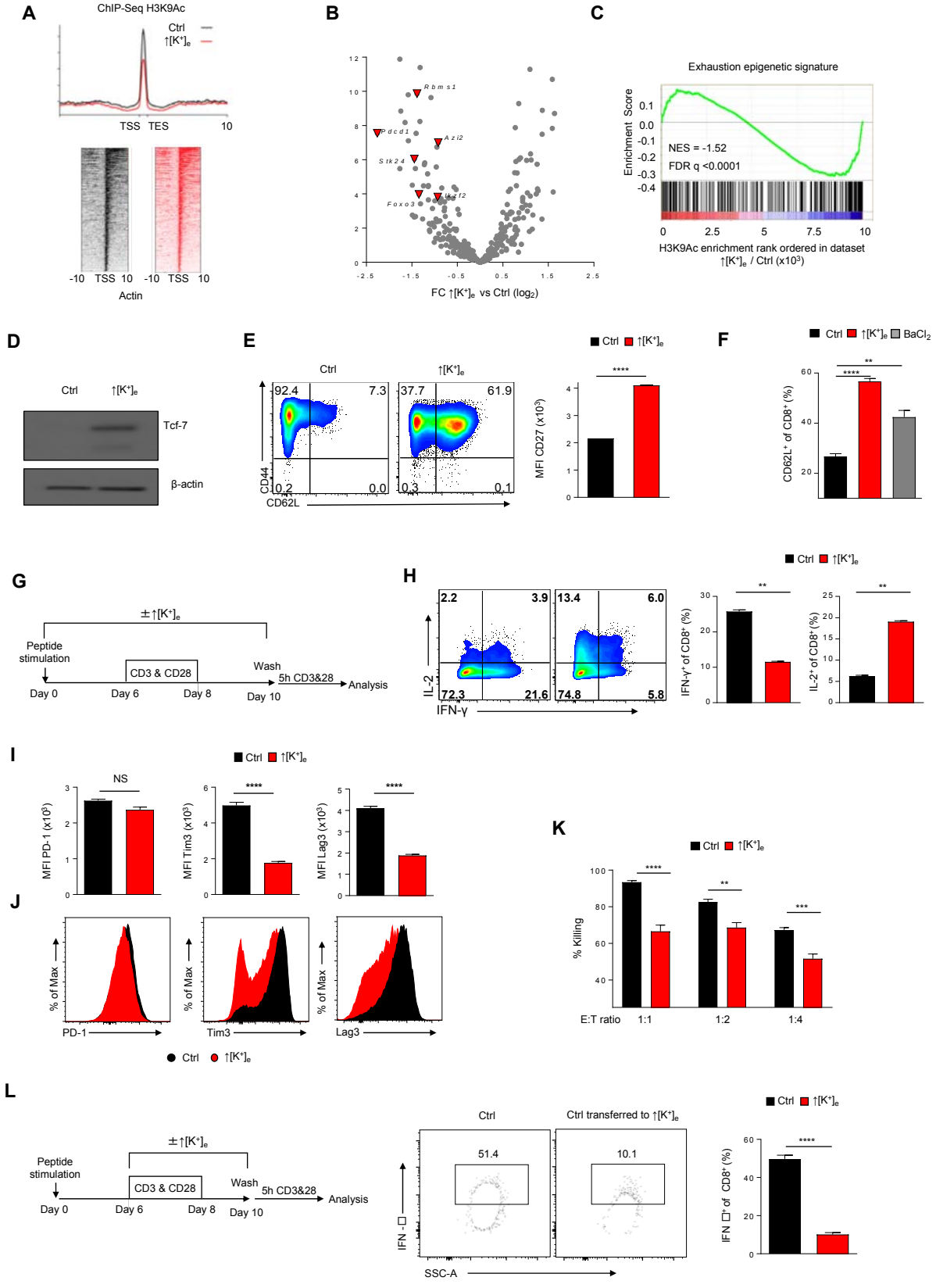
A
ChIP-Seq H3K9Ac
Ctrl
↑[K+]e
TSS TES 10
-10 TSS 10 -10 TSS 10
Actin
B
Rbms1
Pdcd1
Azi2
Stk24
Foxo3
Ikzf2
FC ↑[K+]e vs Ctrl (log2)
C
Exhaustion epigenetic signature
Enrichment Score
NES = -1.52
FDR q <0.0001
H3K9Ac enrichment rank ordered in dataset
↑[K+]e / Ctrl (x10³)
D
Ctrl ↑[K+]e
Tcf-7
β-actin
E
Ctrl ↑[K+]e
92.4 7.3 0.2 0.0
37.7 61.9 0.3 0.1
CD44
CD62L
MFI CD27 (x10³)
F
Ctrl ↑[K+]e BaCl2
CD62L+ of CD8+ (%)
G
±↑[K+]e
Peptide stimulation
CD3 & CD28
Wash
5h CD3&28
Analysis
Day 0 Day 6 Day 8 Day 10
H
2.2 3.9 72.3 21.6
13.4 6.0 74.8 5.8
IL-2
IFN-γ
IFN-γ+ of CD8+ (%)
IL-2+ of CD8+ (%)
I
MFI PD-1 (x10³)
MFI Tim3 (x10³)
MFI Lag3 (x10³)
NS
J
% of Max
PD-1
Tim3
Lag3
K
% Killing
E:T ratio 1:1 1:2 1:4
L
Peptide stimulation
±↑[K+]e
CD3 & CD28
Wash
5h CD3&28
Analysis
Day 0 Day 6 Day 8 Day 10
Ctrl
Ctrl transferred to ↑[K+]e
51.4
10.1
IFN -□
SSC-A
IFN □+ of CD8+ (%)

fig. S5 ↑$[K^+]_e$ limits acquisition of effector functions and maintains $CD8^+$ T cells in a less differentiated state

(**A**) Differentially bound H3K9Ac deposition in ↑$[K^+]_e$ and control cells for effector genes identified in volcano plots of Figure 3H (centered ± 10 kb). (**B**) Volcano plot representing the H3K9Ac deposition at exhaustion genes which were enriched at open chromatin regions from ATAC-seq datasets (GSE86797) (**C**) GSEA showing negative enrichment for the exhausted genes represented in (B). NES, normalized enrichment score; FDR, false discovery rate. **(D)** Immunoblot of stemness associated transcription factor TCF7 in $CD8^+$ T cells cultured in indicated conditions. (**E**) Quantifications showing $CD8^+CD62L^+$ percentages of T cells cultured in indicated conditions **(F)** Quantifications showing $CD8^+CD62L^+$ percentages of $CD8^+$ T cells cultured in non-selective potassium channel inhibitor $BaCl_2$ (2 mM). (**G**) Experimental set-up of *in vitro* culture conditions of pmel $CD8^+$ T cells and activation of T cells for intracellular cytokine analysis. (**H**) Representative flow cytometry plots showing IFN-γ and IL-2 production in the indicated conditions and quantifications of $IL\text{-}2^+$ and $IFN\text{-}\gamma^+$ of $CD8^+$ T cells cultured in control or↑$[K^+]_e$. (**I, J**) Representative FACS histograms and quantification of Pd1, Tim3, Lag3 expression of T cells cultured in indicated conditions. (**K**) Experimental set-up and quantification of killing with pmel $CD8^+$ T cells: B16 gp100 (E:T) in control or↑$[K^+]_e$. (**L**) Schematic showing activation of pmel $CD8^+$ T cells in normal ionic conditions and transferring to ↑$[K^+]$ during secondary stimulation. Representative flow cytometry plots showing % IFN-γ of $CD8^+$ T cell and quantifications showing delayed acquisition of effector functions in activated T cells exposed to ↑$[K^+]_e$. For all relevant figures, data show mean +/- SEM and is representative of at least two or three independent experiments with n = at least three culture replicates, two-tailed t-tests, asterisks indicating significance are * $P < 0.05$; ** $P < 0.01$; *** $P < 0.001$; **** $P < 0.0001$ between selected relevant comparisons.

Fig. S6

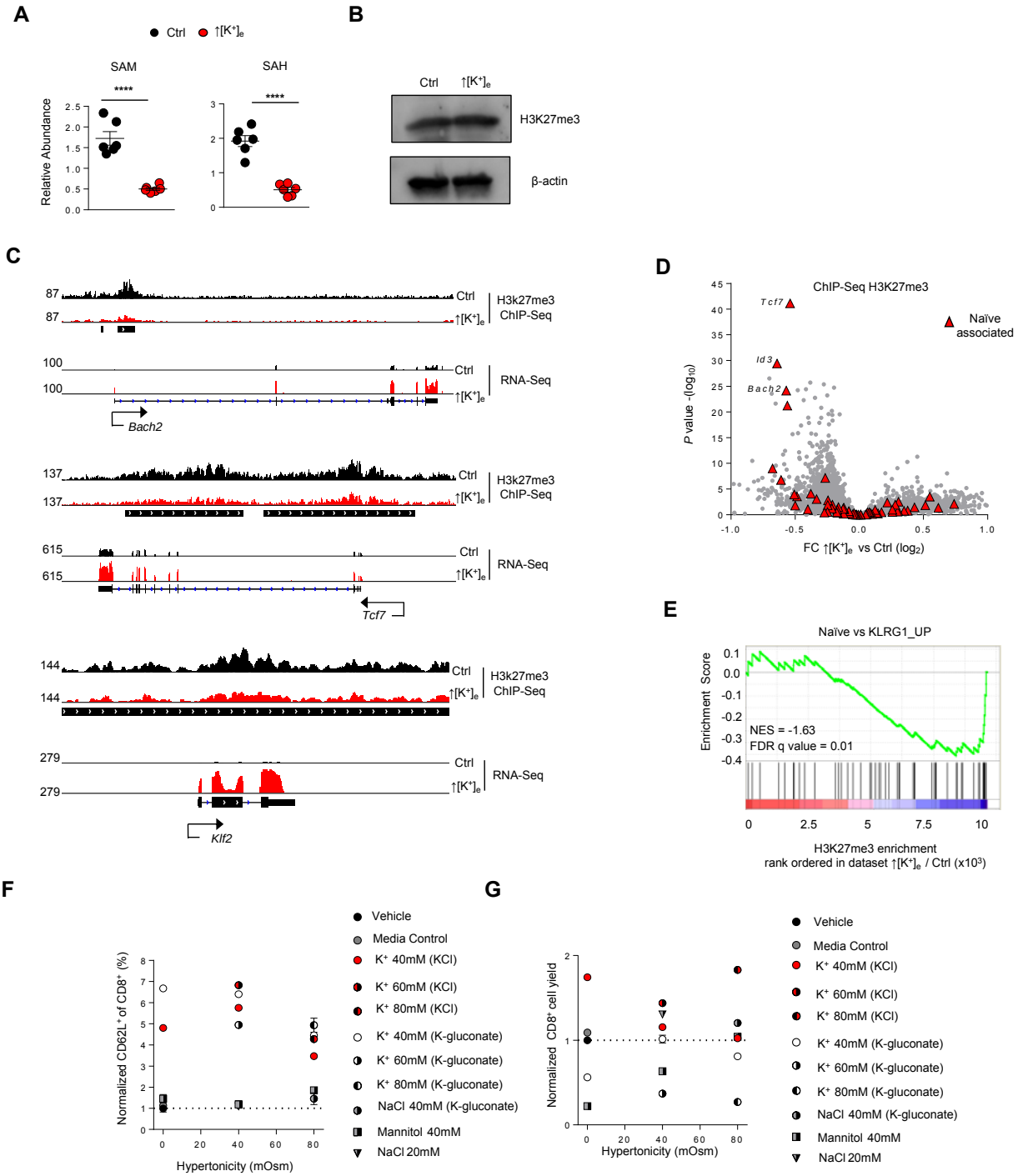
A
Ctrl
↑[K+]e
SAM
SAH
****
Relative Abundance
B
Ctrl
↑[K+]e
H3K27me3
β-actin
C
H3k27me3 ChIP-Seq
RNA-Seq
Bach2
Tcf7
Klf2
D
ChIP-Seq H3K27me3
Naïve associated
Tcf7
Id3
Bach2
P value -(log10)
FC ↑[K+]e vs Ctrl (log2)
E
Naïve vs KLRG1_UP
Enrichment Score
NES = -1.63
FDR q value = 0.01
H3K27me3 enrichment
rank ordered in dataset ↑[K+]e / Ctrl (x10³)
F
Normalized CD62L+ of CD8+ (%)
Hypertonicity (mOsm)
Vehicle
Media Control
K+ 40mM (KCl)
K+ 60mM (KCl)
K+ 80mM (KCl)
K+ 40mM (K-gluconate)
K+ 60mM (K-gluconate)
K+ 80mM (K-gluconate)
NaCl 40mM (K-gluconate)
Mannitol 40mM
NaCl 20mM
G
Normalized CD8+ cell yield
Hypertonicity (mOsm)

fig. S6 ↑$[K^+]_e$ mediated metabolic programming preserves epigenetic stemness
(**A**) Quantification of methionine cycle intermediates SAM and SAH by LC-MS/MS in the indicated conditions (n=6 replicates per condition). (**B**) Representative immunoblots showing total histone lysine 27 (H3K27me3) in indicated conditions. (**C**) Representative genomic alignments of H3K27me3 and RNA-seq measurements showing reduced deposition of methylation or transcripts at the *Bach2*, *Tcf7*, and *Klf2* locus of $CD8^+$ T cells treated in the indicated conditions. Black bars under the tracks represent the called common peaks in ↑$[K^+]$e and control. (**D**) Volcano plot representing a subset of memory associated genes and naïve associated genes with reduced H3K27me3 deposition in ↑$[K^+]$e than control T cells. (**E**) GSEA showing negative enrichment for H3K27me3 within naive associated genes. **(F, G)** Quantifications of normalized CD62L populations and total cellular yields in varying hypertonic or isotonic potassium conditions. For all relevant figures, data show mean +/- SEM and is representative of at least two independent experiments with n = at least three culture replicates, two-tailed t-tests, asterisks indicating significance are * $P < 0.05$; ** $P < 0.01$; *** $P < 0.001$; **** $P < 0.0001$ between selected relevant comparisons.

Fig. S7

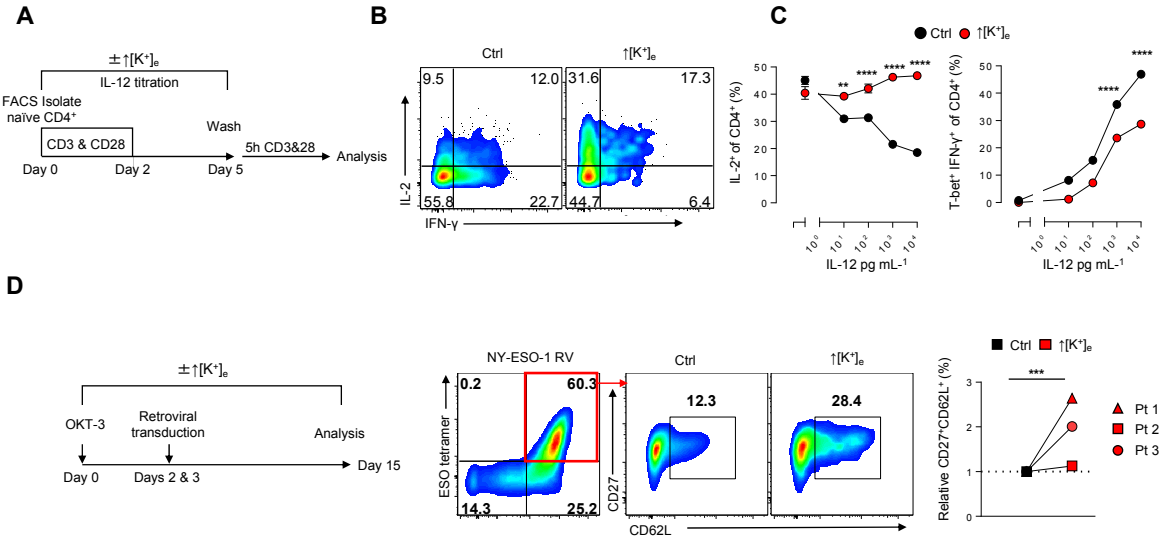

fig. S7 ↑$[K^+]_e$ limits effector cell differentiation of CD4$^+$ and genetically engineered T cells
(**A**) Experimental set-up for activation of naïve CD4$^+$ T cells in the indicated conditions, control or ↑$[K^+]_e$ (↑$[K^+]$e= additional 40 mM). (**B**) Representative flow cytometry plots showing IFN-γ and IL-2 production in the indicated conditions. (**C**) Quantifications of IL-2$^+$ or T-bet$^+$ IFN-γ$^+$ of CD4$^+$ T cells cultured in control or↑$[K^+]_e$ with varying concentrations of IL-12. (**D**) Schematics of the culture conditions and retroviral transduction of T cell with NY-ESO-1 TCR. Representative pseudo color and quantification of CD27$^+$ CD62L$^+$ cells in peripheral blood leukocytes obtained from three melanoma patients transduced with the HLA-A*0201-restricted NY-ESO-1 TCR and cultured in indicated conditions. For all relevant figures, data show mean +/- SEM and is representative of at least two independent experiments with n = at least three culture replicates, two-tailed t-tests, asterisks indicating significance are * $P < 0.05$; ** $P < 0.01$; *** $P < 0.001$; **** $P < 0.0001$ between selected relevant comparisons.

Fig. S8

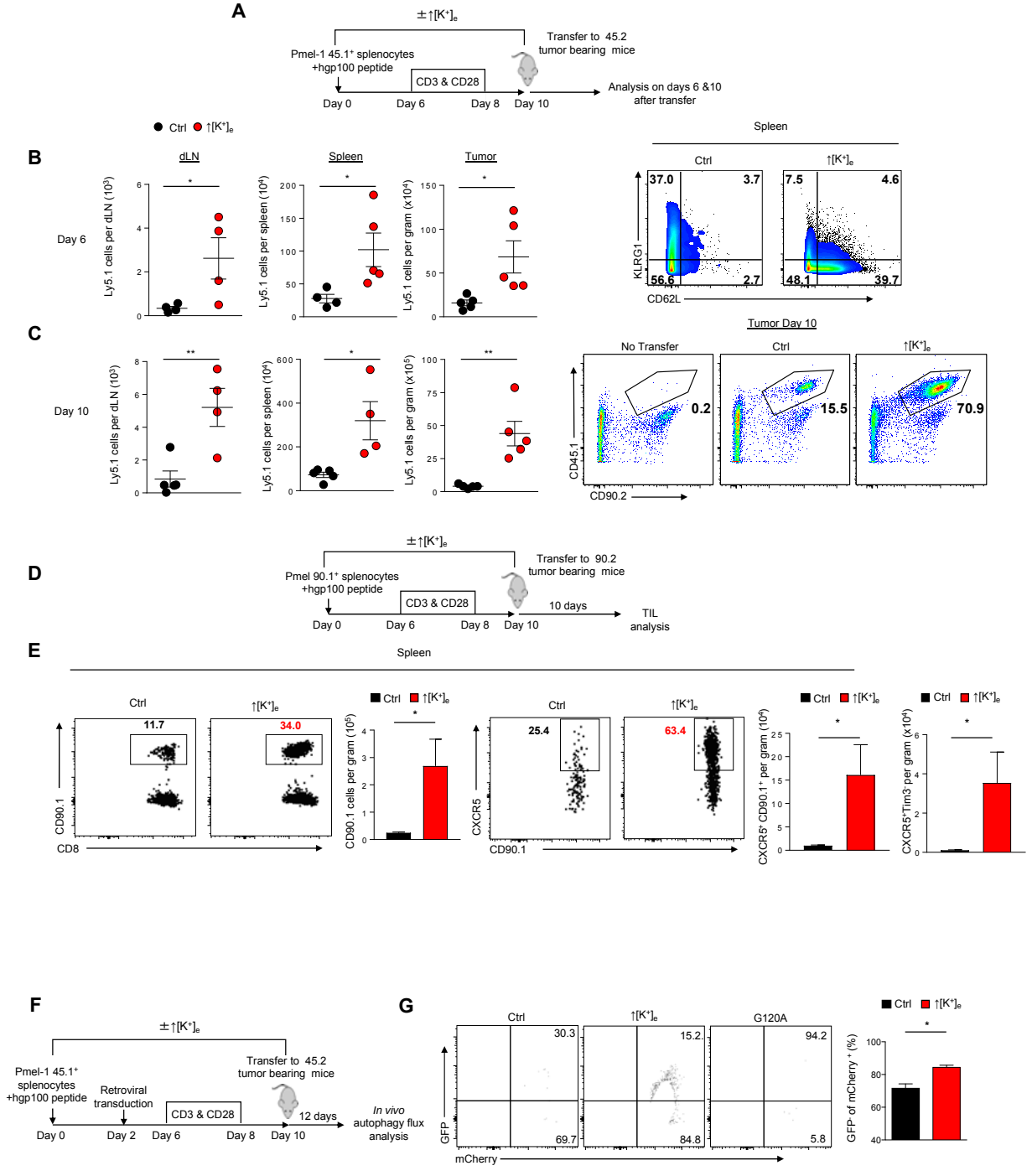
A
±↑[K+]e
Pmel-1 45.1+ splenocytes
+hgp100 peptide
CD3 & CD28
Transfer to 45.2
tumor bearing mice
Analysis on days 6 &10
after transfer
Day 0
Day 6
Day 8
Day 10
Ctrl
↑[K+]e
B
dLN
Spleen
Tumor
Day 6
Ly5.1 cells per dLN (10³)
Ly5.1 cells per spleen (10⁴)
Ly5.1 cells per gram (x10⁴)
Spleen
KLRG1
CD62L
37.0
3.7
56.6
2.7
7.5
4.6
48.1
39.7
C
Day 10
Tumor Day 10
No Transfer
CD45.1
CD90.2
0.2
15.5
70.9
D
Pmel 90.1+ splenocytes
+hgp100 peptide
Transfer to 90.2
tumor bearing mice
10 days
TIL
analysis
E
Spleen
CD90.1
CD8
11.7
34.0
CD90.1 cells per gram (10⁵)
CXCR5
25.4
63.4
CXCR5+ CD90.1+ per gram (10⁴)
CXCR5+Tim3- per gram (x10⁴)
F
Pmel-1 45.1+
splenocytes
+hgp100 peptide
Retroviral
transduction
CD3 & CD28
Transfer to 45.2
tumor bearing mice
12 days
Day 0
Day 2
Day 6
Day 8
Day 10
In vivo
autophagy flux
analysis
G
Ctrl
↑[K+]e
G120A
30.3
15.2
94.2
69.7
84.8
5.8
GFP
mCherry
GFP- of mCherry+ (%)

fig. S8. ↑$[K^+]_e$ promotes persistence and anti-tumor activity of T cells following adoptive transfer

(**A**) Schematic illustrating control or ↑$[K^+]_e$ T cell culture conditions and adoptive T cell transfer into mice bearing established B16 melanoma tumors. Persistence of the transferred T cells were analysed on day 6 and day 10 in the indicated tissues. (**B, C**) Representative FACS plots and quantifications of adoptively transferred ↑$[K^+]_e$ or control T cells gated on $Ly5.1^+$ $CD90.2^+$ in indicated tissues. (Right) Representative FACS plots showing reduced KLRG1 and increased CD62L expression in ↑$[K^+]$-conditioned cells. Data show mean +/- SEM and is representative of two independent experiments with at least 5 mice per group. (**D**) Schematic illustrating control or ↑$[K^+]_e$ T cell culture conditions and adoptive T cell transfer into mice bearing established B16-melanoma tumors. TILs were analysed on day 10. (**E**) Representative FACS plots showing absolute number quantifications and % of $CXCR5^+$ or $CXCR5^+$ $TIM3^-$ of adoptively transferred ↑$[K^+]_e$ or control T cells in spleen. Data show mean +/- SEM and is representative of two independent experiments with at least 5 mice per group (**F**) Schematic illustrating the measurement of in vivo autophagy flux in the setting of adoptive T cell transfer. (**G**) Representative flow cytometry plots and quantification of autophagy flux by measuring the loss of GFP signal within the Thy1.1 populations. Data show mean +/- SEM and is representative of at least two independent experiments, two-tailed t-tests, asterisks indicating significance are * $P < 0.05$; ** $P < 0.01$; *** $P < 0.001$; **** $P < 0.0001$ between selected relevant comparisons.

Fig. S9

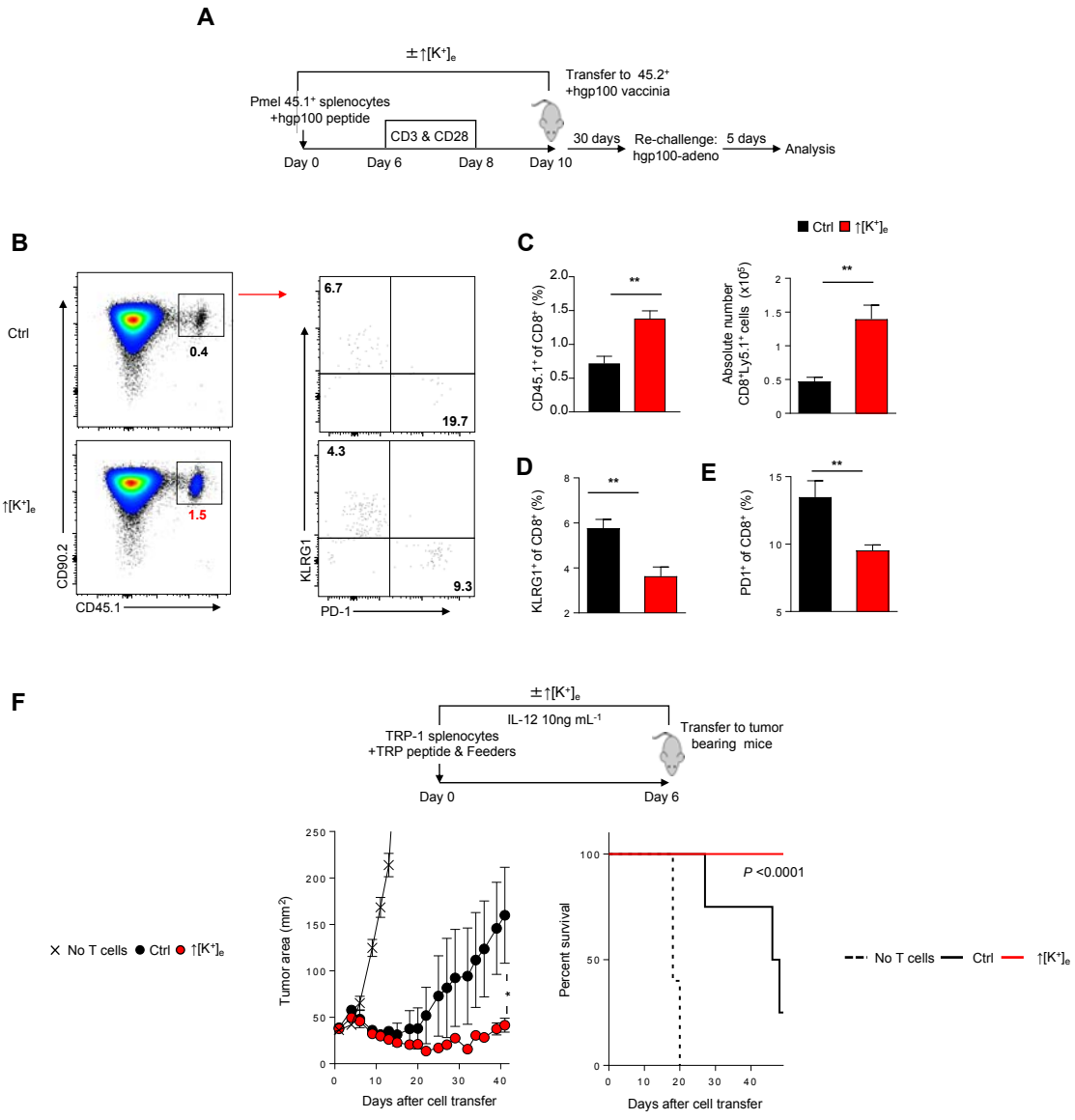
A
±↑[K+]e
Transfer to 45.2+ +hgp100 vaccinia
Pmel 45.1+ splenocytes +hgp100 peptide
CD3 & CD28
Day 0
Day 6
Day 8
Day 10
30 days
Re-challenge: hgp100-adeno
5 days
Analysis
B
Ctrl
↑[K+]e
0.4
1.5
6.7
19.7
4.3
9.3
CD90.2
CD45.1
KLRG1
PD-1
C
Ctrl ↑[K+]e
CD45.1+ of CD8+ (%)
Absolute number CD8+Ly5.1+ cells (x10^5)
D
KLRG1+ of CD8+ (%)
E
PD1+ of CD8+ (%)
F
±↑[K+]e
IL-12 10ng mL-1
TRP-1 splenocytes +TRP peptide & Feeders
Transfer to tumor bearing mice
Day 0
Day 6
× No T cells ● Ctrl ● ↑[K+]e
Tumor area (mm2)
Days after cell transfer
Percent survival
P <0.0001
No T cells Ctrl ↑[K+]e

fig. S9 ↑$[K^+]_e$ conditioning augments *in vivo* recall and anti-tumor activity of adoptively transferred cells.

(A) Schematic illustrating measurement of *in vivo* memory recall responses of control or ↑$[K^+]_e$ T cells in mice challenged with vaccinia virus expressing gp100. Memory recall responses of the transferred T cells (CD45.1) were analysed on day 30 by challenging the hosts (CD45.2) with adenovirus expressing gp100. (**B, C**) Representative FACS plots and quantifications showing percentages and absolute numbers of $CD45.1^+$ of recalled $CD8^+$ T cells 5 days post viral challenge. (**D, E**) Quantifications showing percentages $KLRG1^+$ and $PD1^+$ of recalled $CD8^+$ T cells. Data show mean +/- SEM and is representative of two independent experiments with at least 5 mice per group (**F**) Adoptive T cell therapy and survival rates of sub lethally irradiated mice bearing B16-Trp1 tumors treated with $CD4^+$ TRP-1 transgenic T cell cultured in control or ↑$[K^+]_e$. Data show mean +/- SEM and is representative of two independent experiments with at least 5 mice per group. Tumor measurements were plotted as the mean ± SEM. for each data point, and tumour treatment graphs were compared by using the Wilcoxon rank sum test and analysis of animal survival was assessed using a log-rank test. (**C, D, E**) Data show mean +/- SEM and is representative of at least two independent experiments, two-tailed t-tests, asterisks indicating significance are * $P < 0.05$; ** $P < 0.01$; *** $P < 0.001$; **** $P < 0.0001$ between selected relevant comparisons.

Fig. S10

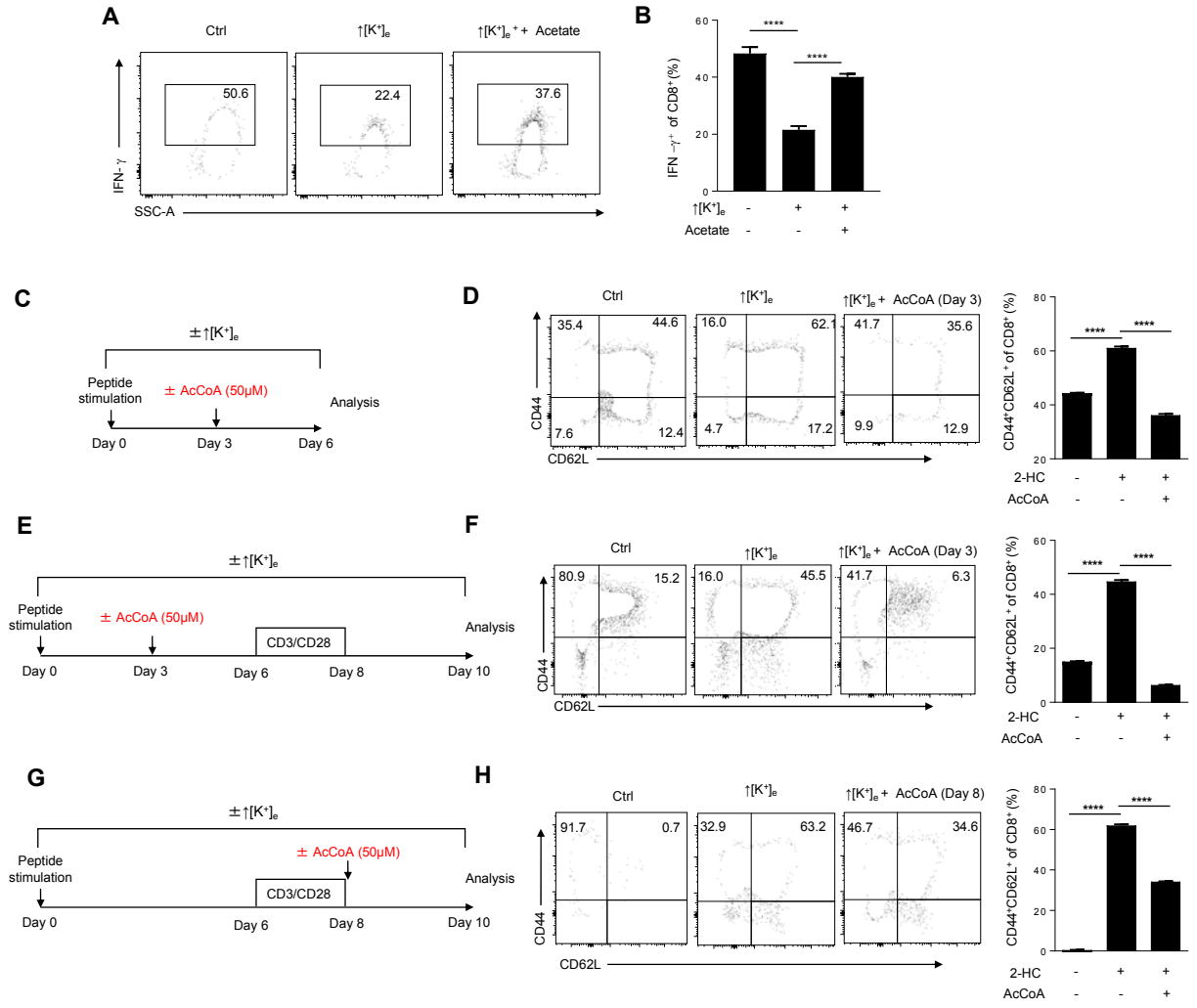

fig. S10. Provision of extracellular acetate or electroporation of AcCoA restores IFNγ production in ↑$[K^+]_e$ exposed $CD8^+$ T cells

(**A, B**) Representative FACS plots and quantification of IFNγ secretion by provision of external acetate in indicated conditions. (**C, E, G**). Experimental set-up of *in vitro* culture conditions of pmel $CD8^+$ T cells with gp100 (10μg/ml) and electroporation of AcCoA (red) on indicated timepoints. All cells were re stimulated on day 6 for 48hrs with CD3,CD28, for a total of 10 day culture in control or ↑$[K^+]_e$ (↑$[K^+]$e= additional 40 mM). (**D, F, H**) Representative flow cytometry analysis and quantification of CD62L vs CD44 positive cells in the indicated conditions. For all relevant figures, data show mean +/- SEM and is representative of at least two independent experiments with n = at least three culture replicates, two-tailed t-tests, asterisks indicating significance are * $P < 0.05$; ** $P < 0.01$; *** $P < 0.001$; **** $P < 0.0001$ between selected relevant comparisons.

Fig. S11

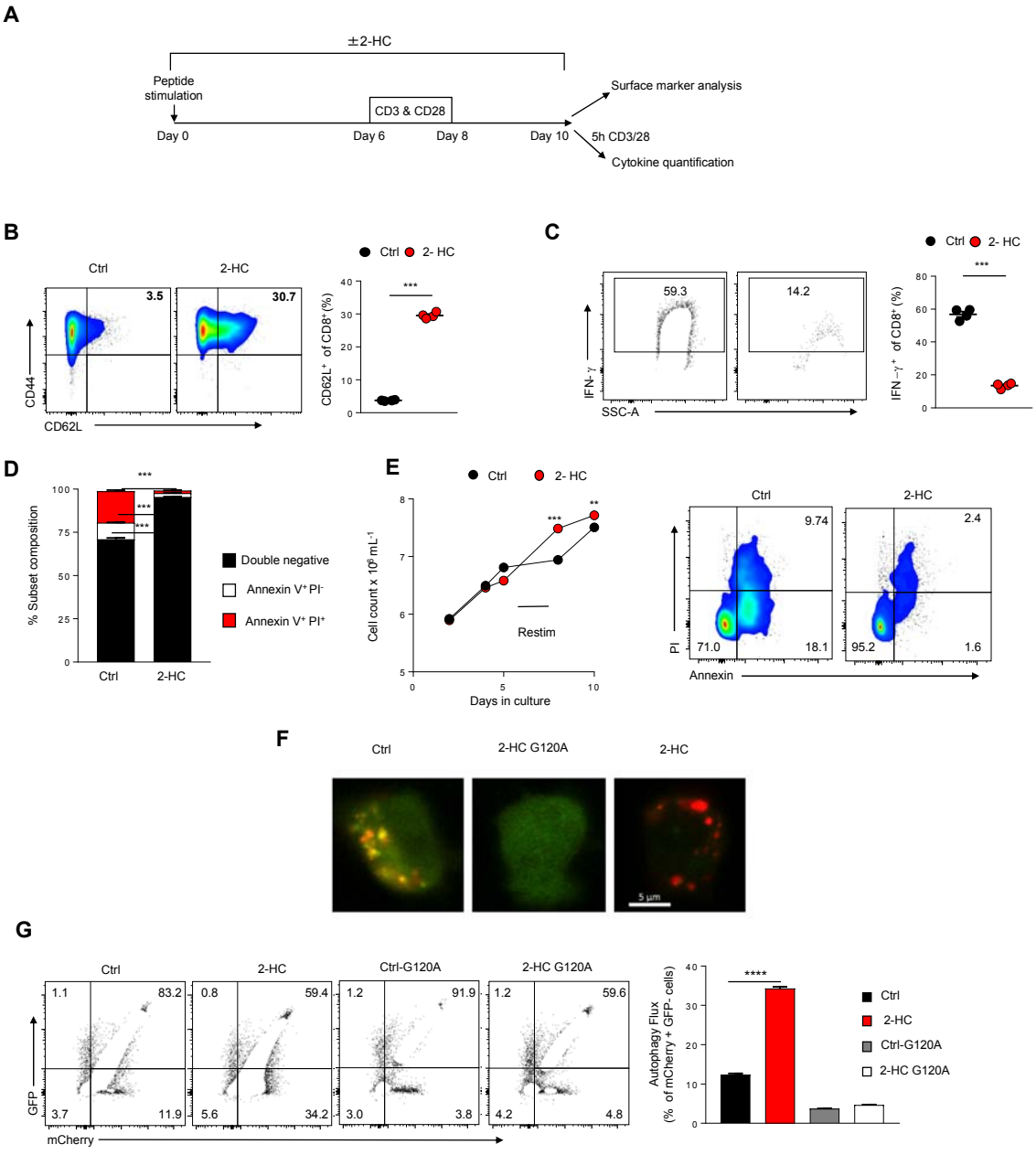
A
±2-HC
Peptide stimulation
CD3 & CD28
Surface marker analysis
Day 0
Day 6
Day 8
Day 10
5h CD3/28
Cytokine quantification
B
Ctrl
2-HC
3.5
30.7
CD44
CD62L
Ctrl
2- HC
CD62L+ of CD8+ (%)
***
C
59.3
14.2
IFN-γ
SSC-A
IFN –γ+ of CD8+ (%)
D
% Subset composition
Double negative
Annexin V+ PI-
Annexin V+ PI+
E
Cell count x 10⁶ mL⁻¹
Restim
Days in culture
9.74
2.4
71.0
18.1
95.2
1.6
PI
Annexin
F
Ctrl
2-HC G120A
2-HC
5 µm
G
Ctrl-G120A
2-HC G120A
1.1
83.2
3.7
11.9
0.8
59.4
5.6
34.2
1.2
91.9
3.0
3.8
1.2
59.6
4.2
4.8
GFP
mCherry
Autophagy Flux
(% of mCherry+ GFP- cells)
****

fig. S11. Treatment with 2-HC limits effector differentiation and promotes autophagy.
(**A**) Schematic of control or 2-hydroxy citrate (2-HC) T cell culture conditions. $CD8^+$ Pmel-1 T cells were activated with gp100 peptide for 5 days in the presence of 5mM 2-HC followed by secondary stimulation with anti-CD3 (1 μg/ml) and anti-CD28 (1 μg/ml). Cells were analysed for surface markers or intracellular cytokines on day 10. (**B, C**) Representative flow cytometry analysis and quantification of CD62L vs CD44 positive cells and IFN-γ production in T cells cultured in control or (2-HC-5mM). (**D)** Representative FACS plots defining the percentages of live (Annexin V^- PI^-), apoptotic (Annexin V^+PI^-) and necrotic populations (Annexin V^+ $PI^{+)}$ cultured in control or 2-HC. (**E**) Absolute $CD8^+$ T cell numbers quantification over the course of culture. (**F**) Representative live cell confocal images defining the GFP and mCherry puncta in cells treated under indicated conditions. (**G**) Representative flow cytometry plots and quantification of autophagy flux by measuring the loss of GFP signal and accumulation of mCherry using flow cytometry in indicated conditions. For all relevant figures data show mean +/- SEM and is representative of at least two independent experiments with n = at least three culture replicates(B,C,D,G), two-tailed t-tests, asterisks indicating significance are * $P < 0.05$; ** $P < 0.01$; *** $P < 0.001$; **** $P < 0.0001$ between selected relevant comparisons.

Fig. S12

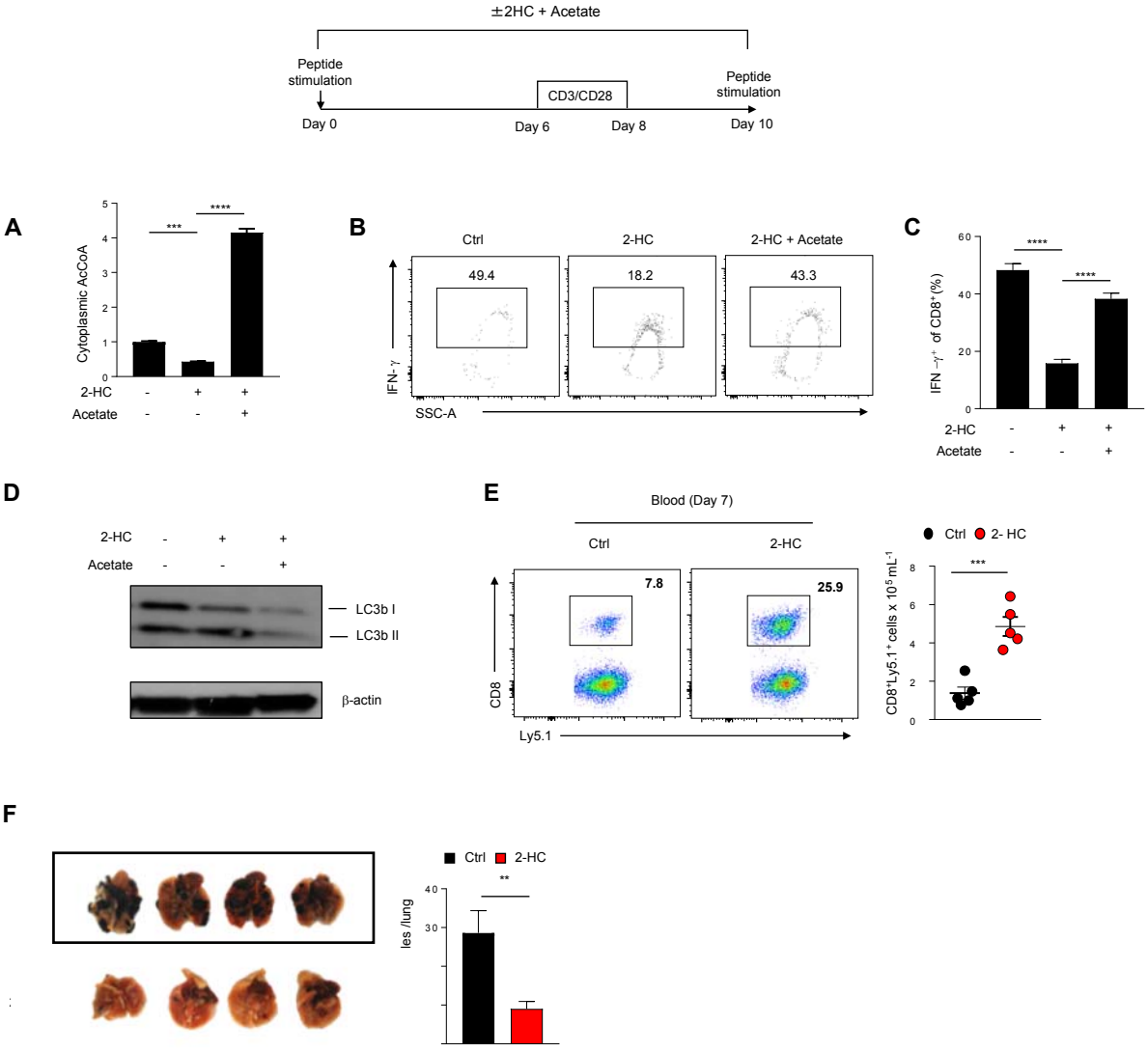
±2HC + Acetate
Peptide stimulation
CD3/CD28
Peptide stimulation
Day 0
Day 6
Day 8
Day 10
A
Cytoplasmic AcCoA
2-HC
Acetate
B
Ctrl
2-HC
2-HC + Acetate
49.4
18.2
43.3
IFN- γ
SSC-A
C
IFN –γ+ of CD8+(%)
2-HC
Acetate
D
2-HC
Acetate
LC3b I
LC3b II
β-actin
E
Blood (Day 7)
Ctrl
2-HC
7.8
25.9
CD8
Ly5.1
Ctrl
2- HC
CD8+Ly5.1+ cells x 10^5 mL-1
F
Ctrl
2-HC
les /lung

fig. S12. Provision of acetate restores AcCoA levels and IFNγ production of 2-HC treated $CD8^+$ T cells

(**A**) Restoration of cytoplasmic AcCoA by provision of external acetate (Acetate-5mM) in the indicated conditions. (**B, C**) Representative FACS plots and quantification of IFNγ secretion by provision of external acetate in indicated conditions. (**D**) Immunoblot showing ablation of autophagy in 2-HC by provision of external acetate. (**E**) Representative FACS plots and quantification of adoptively transferred control or 2-HC T cells gated on $CD8^+Ly5.1^+$. Recall responses were performed by challenging the mice with 1×10^7 plaque-forming units (PFU) vaccinia virus expressing gp100. Absolute numbers were quantified in the blood on day 7 post adoptive T cell transfer. (**F**) Representative images of B16-F10 lung metastatic nodules and quantification 14 days post treatment with control (n=10) or 2-HC (n=10) treated T cells. For all relevant figures data show mean +/- SEM and is representative of at least two independent experiments, two-tailed t-tests, asterisks indicating significance are * $P < 0.05$; ** $P < 0.01$; *** $P < 0.001$; **** $P < 0.0001$ between selected relevant comparisons.

Fig. S13

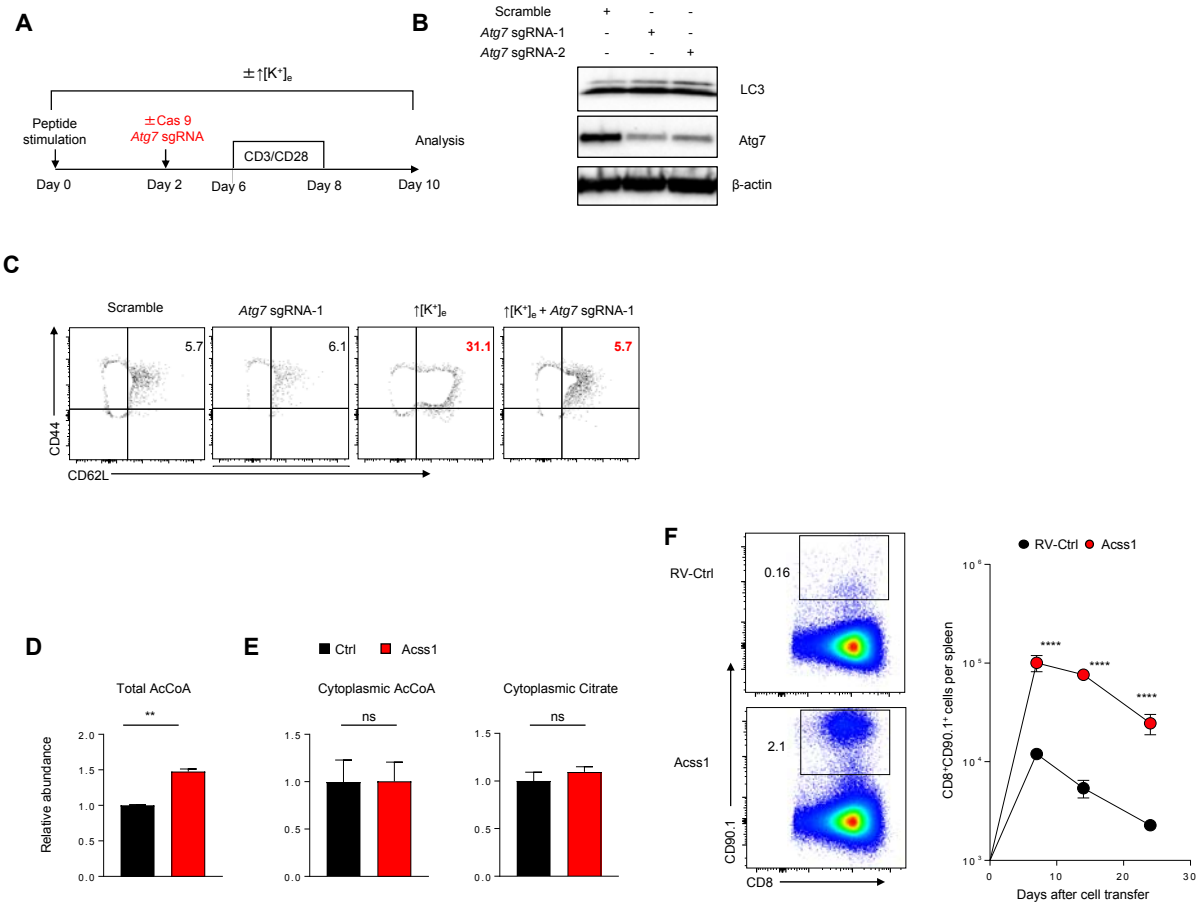
A
±↑[K+]e
Peptide stimulation
±Cas 9
Atg7 sgRNA
CD3/CD28
Analysis
Day 0
Day 2
Day 6
Day 8
Day 10
B
Scramble + - -
Atg7 sgRNA-1 - + -
Atg7 sgRNA-2 - - +
LC3
Atg7
β-actin
C
Scramble
Atg7 sgRNA-1
↑[K+]e
↑[K+]e + Atg7 sgRNA-1
5.7
6.1
31.1
5.7
CD44
CD62L
D
Total AcCoA
**
Relative abundance
E
Ctrl
Acss1
Cytoplasmic AcCoA
ns
Cytoplasmic Citrate
ns
F
RV-Ctrl
0.16
Acss1
2.1
CD90.1
CD8
RV-Ctrl
Acss1
CD8+CD90.1+ cells per spleen
****
****
****
Days after cell transfer

fig. S13. Autophagy is critical for preserved stemness following ↑[K^+]e

(**A**) Experimental set-up of *in vitro* culture conditions of pmel $CD8^+$ T cells with gp100 (10μg/ml) and electroporation of CAS9 protein and Atg7-targeting sgRNAs on indicated timepoints. All cells were re stimulated on day 6 for 48hrs with CD3,CD28, for a total of 10 day culture in control or ↑$[K^+]_e$ (↑$[K^+]$e= additional 40 mM). (**B**) Immunoblots showing reduction in ATG7 protein and ablation of autophagy in ↑$[K^+]_e$ conditions. (**C**) Representative flow cytometry analysis showing reduction in CD62Lpositive cells in the setting of ↑$[K^+]_e$ and ATG7 disruption. Statistics in Fig.5Q. (**D**) Quantifications of total cellular AcCoA. **(E)** cytoplasmic AcCoA and cytoplasmic citrate from the cells treated in the indicated condition. (**D, E**) Data show mean +/- SEM and is representative of at least two independent experiments with n = at least three culture replicates, two-tailed t-tests. (**F**) Representative flow cytometry analysis (left) and absolute number quantification (right) of RV-control or Acss1-Thy1.1 of transferred cells in the spleen 7, 14, 21 days post adoptive transfer by challenging with recombinant vaccinia virus expressing gp100. *In vivo* data shown are representative of two independent experiments with at least 5 mice per group. Data show mean +/- SEM and is representative of at least two independent experiments, two-tailed t-tests, asterisks indicating significance are * $P < 0.05$; ** $P < 0.01$; *** $P < 0.001$; **** $P < 0.0001$ between selected relevant comparisons.

Fig. S14

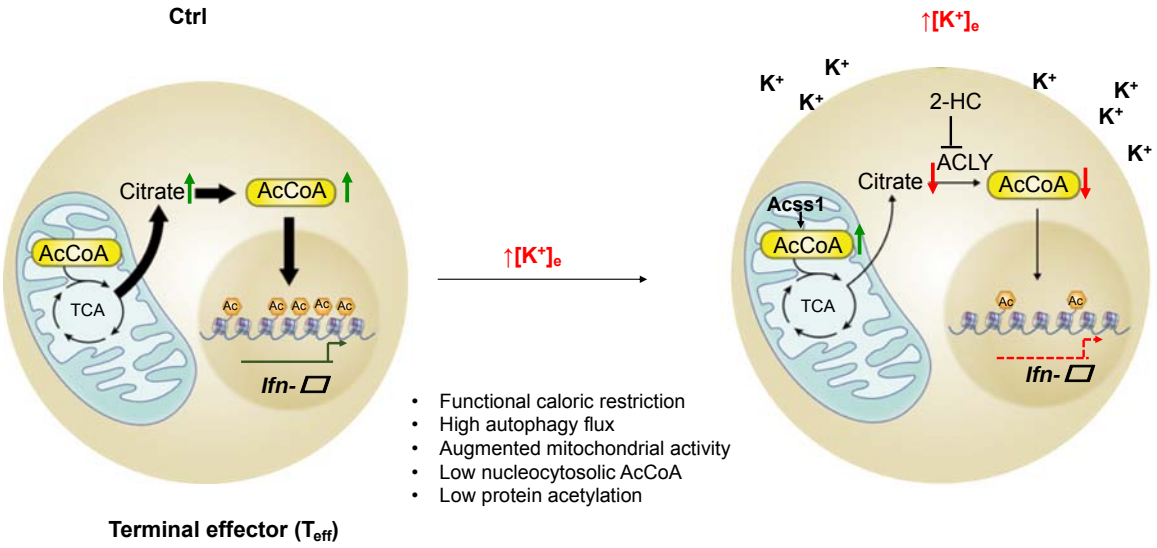

fig. S14. A model depicting the dynamic link between local ions, metabolite abundance and epigenetic status in $CD8^+$ T cells.

References

1. S. A. Rosenberg, N. P. Restifo, Adoptive cell transfer as personalized immunotherapy for human cancer. *Science* **348**, 62–68 (2015). doi:10.1126/science.aaa4967 Medline

2. M. E. Dudley, J. R. Wunderlich, P. F. Robbins, J. C. Yang, P. Hwu, D. J. Schwartzentruber, S. L. Topalian, R. Sherry, N. P. Restifo, A. M. Hubicki, M. R. Robinson, M. Raffeld, P. Duray, C. A. Seipp, L. Rogers-Freezer, K. E. Morton, S. A. Mavroukakis, D. E. White, S. A. Rosenberg, Cancer regression and autoimmunity in patients after clonal repopulation with antitumor lymphocytes. *Science* **298**, 850–854 (2002). doi:10.1126/science.1076514 Medline

3. S. A. Rosenberg, J. C. Yang, R. M. Sherry, U. S. Kammula, M. S. Hughes, G. Q. Phan, D. E. Citrin, N. P. Restifo, P. F. Robbins, J. R. Wunderlich, K. E. Morton, C. M. Laurencot, S. M. Steinberg, D. E. White, M. E. Dudley, Durable complete responses in heavily pretreated patients with metastatic melanoma using T-cell transfer immunotherapy. *Clin. Cancer Res.* **17**, 4550–4557 (2011). doi:10.1158/1078-0432.CCR-11-0116 Medline

4. N. Zacharakis, H. Chinnasamy, M. Black, H. Xu, Y.-C. Lu, Z. Zheng, A. Pasetto, M. Langhan, T. Shelton, T. Prickett, J. Gartner, L. Jia, K. Trebska-McGowan, R. P. Somerville, P. F. Robbins, S. A. Rosenberg, S. L. Goff, S. A. Feldman, Immune recognition of somatic mutations leading to complete durable regression in metastatic breast cancer. *Nat. Med.* **24**, 724–730 (2018). doi:10.1038/s41591-018-0040-8 Medline

5. A. Ribas, J. D. Wolchok, Cancer immunotherapy using checkpoint blockade. *Science* **359**, 1350–1355 (2018). doi:10.1126/science.aar4060

6. S. Naik, S. B. Larsen, C. J. Cowley, E. Fuchs, Two to Tango: Dialog between Immunity and Stem Cells in Health and Disease. *Cell* **175**, 908–920 (2018). doi:10.1016/j.cell.2018.08.071 Medline

7. H. Gehart, H. Clevers, Tales from the crypt: New insights into intestinal stem cells. *Nat. Rev. Gastroenterol. Hepatol.* **16**, 19–34 (2019). doi:10.1038/s41575-018-0081-y Medline

8. L. Gattinoni, X.-S. Zhong, D. C. Palmer, Y. Ji, C. S. Hinrichs, Z. Yu, C. Wrzesinski, A. Boni, L. Cassard, L. M. Garvin, C. M. Paulos, P. Muranski, N. P. Restifo, Wnt signaling arrests effector T cell differentiation and generates $CD8^+$ memory stem cells. *Nat. Med.* **15**, 808–813 (2009). doi:10.1038/nm.1982 Medline

9. L. Gattinoni, E. Lugli, Y. Ji, Z. Pos, C. M. Paulos, M. F. Quigley, J. R. Almeida, E. Gostick, Z. Yu, C. Carpenito, E. Wang, D. C. Douek, D. A. Price, C. H. June, F. M. Marincola, M. Roederer, N. P. Restifo, A human memory T cell subset with stem cell-like properties. *Nat. Med.* **17**, 1290–1297 (2011). doi:10.1038/nm.2446 Medline

10. N. P. Restifo, L. Gattinoni, Lineage relationship of effector and memory T cells. *Curr. Opin. Immunol.* **25**, 556–563 (2013). doi:10.1016/j.coi.2013.09.003 Medline

11. M. Sade-Feldman, K. Yizhak, S. L. Bjorgaard, J. P. Ray, C. G. de Boer, R. W. Jenkins, D. J. Lieb, J. H. Chen, D. T. Frederick, M. Barzily-Rokni, S. S. Freeman, A. Reuben, P. J. Hoover, A.-C. Villani, E. Ivanova, A. Portell, P. H. Lizotte, A. R. Aref, J.-P. Eliane, M. R. Hammond, H. Vitzthum, S. M. Blackmon, B. Li, V. Gopalakrishnan, S. M. Reddy, Z. A. Cooper, C. P. Paweletz, D. A. Barbie, A. Stemmer-Rachamimov, K. T. Flaherty, J. A. Wargo, G. M. Boland, R. J. Sullivan, G. Getz, N. Hacohen, Defining T Cell States Associated with Response to Checkpoint Immunotherapy in Melanoma. *Cell* **175**, 998–1013.e20 (2018). doi:10.1016/j.cell.2018.10.038 Medline

12. M. Philip, L. Fairchild, L. Sun, E. L. Horste, S. Camara, M. Shakiba, A. C. Scott, A. Viale, P. Lauer, T. Merghoub, M. D. Hellmann, J. D. Wolchok, C. S. Leslie, A. Schietinger, Chromatin states define tumour-specific T cell dysfunction and reprogramming. *Nature* **545**, 452–456 (2017). doi:10.1038/nature22367 Medline

13. S. Kurtulus, A. Madi, G. Escobar, M. Klapholz, J. Nyman, E. Christian, M. Pawlak, D. Dionne, J. Xia, O. Rozenblatt-Rosen, V. K. Kuchroo, A. Regev, A. C. Anderson, Checkpoint Blockade Immunotherapy Induces Dynamic Changes in PD-1^{-}CD8^{+} Tumor-Infiltrating T Cells. *Immunity* **50**, 181–194.e6 (2019). doi:10.1016/j.immuni.2018.11.014 Medline

14. I. Siddiqui, K. Schaeuble, V. Chennupati, S. A. Fuertes Marraco, S. Calderon-Copete, D. Pais Ferreira, S. J. Carmona, L. Scarpellino, D. Gfeller, S. Pradervand, S. A. Luther, D. E. Speiser, W. Held, Intratumoral Tcf1^{+}PD-1^{+}CD8^{+} T Cells with Stem-like Properties Promote Tumor Control in Response to Vaccination and Checkpoint Blockade Immunotherapy. *Immunity* **50**, 195–211.e10 (2019). doi:10.1016/j.immuni.2018.12.021 Medline

15. S. J. Im, M. Hashimoto, M. Y. Gerner, J. Lee, H. T. Kissick, M. C. Burger, Q. Shan, J. S. Hale, J. Lee, T. H. Nasti, A. H. Sharpe, G. J. Freeman, R. N. Germain, H. I. Nakaya, H.-H. Xue, R. Ahmed, Defining CD8^{+} T cells that provide the proliferative burst after PD-1 therapy. *Nature* **537**, 417–421 (2016). doi:10.1038/nature19330 Medline

16. J. G. Crompton, M. Narayanan, S. Cuddapah, R. Roychoudhuri, Y. Ji, W. Yang, S. J. Patel, M. Sukumar, D. C. Palmer, W. Peng, E. Wang, F. M. Marincola, C. A. Klebanoff, K. Zhao, J. S. Tsang, L. Gattinoni, N. P. Restifo, Lineage relationship of CD8^{+} T cell subsets is revealed by progressive changes in the epigenetic landscape. *Cell. Mol. Immunol.* **13**, 502–513 (2016). doi:10.1038/cmi.2015.32 Medline

17. H. Chi, Regulation and function of mTOR signalling in T cell fate decisions. *Nat. Rev. Immunol.* **12**, 325–338 (2012). doi:10.1038/nri3198 Medline

18. R. J. Kishton, M. Sukumar, N. P. Restifo, Metabolic Regulation of T Cell Longevity and Function in Tumor Immunotherapy. *Cell Metab.* **26**, 94–109 (2017). doi:10.1016/j.cmet.2017.06.016 Medline

19. H. Lodish, A. Berk, S. Zipursky, in *Molecular Cell Biology, 4th Edition* (2000), pp. 1–5.

20. R. G. Ladstein, I. M. Bachmann, O. Straume, L. A. Akslen, Tumor necrosis is a prognostic factor in thick cutaneous melanoma. *Am. J. Surg. Pathol.* **36**, 1477–1482 (2012). doi:10.1097/PAS.0b013e31825a5b45 Medline

21. K. Komori, Y. Kanemitsu, K. Kimura, N. Hattori, T. Sano, S. Ito, T. Abe, Y. Senda, K. Misawa, Y. Ito, N. Uemura, Y. Shimizu, Tumor necrosis in patients with TNM stage IV colorectal cancer without residual disease (R0 Status) is associated with a poor prognosis. *Anticancer Res.* **33**, 1099–1105 (2013). Medline

22. R. Eil, S. K. Vodnala, D. Clever, C. A. Klebanoff, M. Sukumar, J. H. Pan, D. C. Palmer, A. Gros, T. N. Yamamoto, S. J. Patel, G. C. Guittard, Z. Yu, V. Carbonaro, K. Okkenhaug, D. S. Schrump, W. M. Linehan, R. Roychoudhuri, N. P. Restifo, Ionic immune suppression within the tumour microenvironment limits T cell effector function. *Nature* **537**, 539–543 (2016). doi:10.1038/nature19364 Medline

23. L. Gattinoni, C. A. Klebanoff, N. P. Restifo, Paths to stemness: Building the ultimate antitumour T cell. *Nat. Rev. Cancer* **12**, 671–684 (2012). doi:10.1038/nrc3322 Medline

24. J. A. Schafer, E. Heinz, The effect of reversal on Na^+ and K^+ electrochemical potential gradients on the active transport of amino acids in Ehrlich ascites tumor cells. *Biochim. Biophys. Acta* **249**, 15–33 (1971). doi:10.1016/0005-2736(71)90079-4 Medline

25. A. A. Eddy, M. F. Mulcahy, P. J. Thomson, The effects of sodium ions and potassium ions on glycine uptake by mouse ascites-tumour cells in the presence and absence of selected metabolic inhibitors. *Biochem. J.* **103**, 863–876 (1967). doi:10.1042/bj1030863 Medline

26. C. J. Cummins, R. A. Glover, O. Z. Sellinger, Potassium modulation of methionine uptake in astrocytes in vitro. *Neurochem. Res.* **7**, 637–644 (1982). doi:10.1007/BF00965129 Medline

27. M. Levite, L. Cahalon, A. Peretz, R. Hershkoviz, A. Sobko, A. Ariel, R. Desai, B. Attali, O. Lider, Extracellular K^+ and opening of voltage-gated potassium channels activate T cell integrin function: Physical and functional association between Kv1.3 channels and beta1 integrins. *J. Exp. Med.* **191**, 1167–1176 (2000). doi:10.1084/jem.191.7.1167 Medline

28. F. Gibellini, T. K. Smith, The Kennedy pathway—De novo synthesis of phosphatidylethanolamine and phosphatidylcholine. *IUBMB Life* **62**, 414–428 (2010). doi:10.1002/iub.354 Medline

29. X. Xu, K. Araki, S. Li, J.-H. Han, L. Ye, W. G. Tan, B. T. Konieczny, M. W. Bruinsma, J. Martinez, E. L. Pearce, D. R. Green, D. P. Jones, H. W. Virgin, R. Ahmed, Autophagy is essential for effector $CD8^+$ T cell survival and memory formation. *Nat. Immunol.* **15**, 1152–1161 (2014). doi:10.1038/ni.3025 Medline

30. D. J. Klionsky *et al*., Guidelines for the use and interpretation of assays for monitoring autophagy. *Autophagy* **12**, 1–222 (2012). doi:10.4161/auto.19496 Medline

31. F. Pietrocola, L. Galluzzi, J. M. Bravo-San Pedro, F. Madeo, G. Kroemer, Acetyl coenzyme A: A central metabolite and second messenger. *Cell Metab.* **21**, 805–821 (2015). doi:10.1016/j.cmet.2015.05.014 Medline

32. K. J. Menzies, H. Zhang, E. Katsyuba, J. Auwerx, Protein acetylation in metabolism - metabolites and cofactors. *Nat. Rev. Endocrinol.* **12**, 43–60 (2016). doi:10.1038/nrendo.2015.181 Medline

33. B. T. Weinert, V. Iesmantavicius, T. Moustafa, C. Schölz, S. A. Wagner, C. Magnes, R. Zechner, C. Choudhary, Acetylation dynamics and stoichiometry in Saccharomyces cerevisiae. *Mol. Syst. Biol.* **10**, 716 (2014). doi:10.1002/msb.134766 Medline

34. A. Drazic, L. M. Myklebust, R. Ree, T. Arnesen, The world of protein acetylation. *Biochim. Biophys. Acta* **1864**, 1372–1401 (2016). doi:10.1016/j.bbapap.2016.06.007 Medline

35. I. G. Denisov, S. G. Sligar, A novel type of allosteric regulation: Functional cooperativity in monomeric proteins. *Arch. Biochem. Biophys.* **519**, 91–102 (2012). doi:10.1016/j.abb.2011.12.017 Medline

36. R. A. Henry, Y.-M. M. Kuo, V. Bhattacharjee, T. J. Yen, A. J. Andrews, Changing the selectivity of p300 by acetyl-CoA modulation of histone acetylation. *ACS Chem. Biol.* **10**, 146–156 (2015). doi:10.1021/cb500726b Medline

37. K. E. Pauken, M. A. Sammons, P. M. Odorizzi, S. Manne, J. Godec, O. Khan, A. M. Drake, Z. Chen, D. R. Sen, M. Kurachi, R. A. Barnitz, C. Bartman, B. Bengsch, A. C. Huang, J. M. Schenkel, G. Vahedi, W. N. Haining, S. L. Berger, E. J. Wherry, Epigenetic stability of exhausted T cells limits durability of reinvigoration by PD-1 blockade. *Science* **354**, 1160–1165 (2016). doi:10.1126/science.aaf2807

38. E. Azizi, A. J. Carr, G. Plitas, A. E. Cornish, C. Konopacki, S. Prabhakaran, J. Nainys, K. Wu, V. Kiseliovas, M. Setty, K. Choi, R. M. Fromme, P. Dao, P. T. McKenney, R. C. Wasti, K. Kadaveru, L. Mazutis, A. Y. Rudensky, D. Pe'er, Single-Cell Map of Diverse Immune Phenotypes in the Breast Tumor Microenvironment. *Cell* **174**, 1293–1308.e36 (2018). doi:10.1016/j.cell.2018.05.060 Medline

39. S. M. Gray, R. A. Amezquita, T. Guan, S. H. Kleinstein, S. M. Kaech, Polycomb Repressive Complex 2-Mediated Chromatin Repression Guides Effector $CD8^+$ T Cell Terminal Differentiation and Loss of Multipotency. *Immunity* **46**, 596–608 (2017). doi:10.1016/j.immuni.2017.03.012 Medline

40. M. Peng, N. Yin, S. Chhangawala, K. Xu, C. S. Leslie, M. O. Li, Aerobic glycolysis promotes T helper 1 cell differentiation through an epigenetic mechanism. *Science* **354**, 481–484 (2016). doi:10.1126/science.aaf6284 Medline

41. M. L. L. Balmer, E. H. Ma, G. R. Bantug, J. Grählert, S. Pfister, T. Glatter, A. Jauch, S. Dimeloe, E. Slack, P. Dehio, M. A. Krzyzaniak, C. G. King, A.-V. Burgener, M. Fischer, L. Develioglu, R. Belle, M. Recher, W. V. Bonilla, A. J. Macpherson, S. Hapfelmeier, R. G. Jones, C. Hess, Memory $CD8^+$ T Cells Require Increased Concentrations of Acetate Induced by Stress for Optimal Function. *Immunity* **44**, 1312–1324 (2016). doi:10.1016/j.immuni.2016.03.016 Medline

42. F. Pietrocola, J. Pol, E. Vacchelli, S. Rao, D. P. Enot, E. E. Baracco, S. Levesque, F. Castoldi, N. Jacquelot, T. Yamazaki, L. Senovilla, G. Marino, F. Aranda, S. Durand, V. Sica, A. Chery, S. Lachkar, V. Sigl, N. Bloy, A. Buque, S. Falzoni, B. Ryffel, L. Apetoh, F. Di Virgilio, F. Madeo, M. C. Maiuri, L. Zitvogel, B. Levine, J. M. Penninger, G. Kroemer, Caloric Restriction Mimetics Enhance Anticancer Immunosurveillance. *Cancer Cell* **30**, 147–160 (2016). doi:10.1016/j.ccell.2016.05.016 Medline

43. A. J. Lakhter, J. Hamilton, R. L. Konger, N. Brustovetsky, H. E. Broxmeyer, S. R. Naidu, Glucose-independent Acetate Metabolism Promotes Melanoma Cell Survival and Tumor Growth. *J. Biol. Chem.* **291**, 21869–21879 (2016). doi:10.1074/jbc.M115.712166 Medline

44. X. Liu, D. E. Cooper, A. A. Cluntun, M. O. Warmoes, S. Zhao, M. A. Reid, J. Liu, P. J. Lund, M. Lopes, B. A. Garcia, K. E. Wellen, D. G. Kirsch, J. W. Locasale, Acetate Production from Glucose and Coupling to Mitochondrial Metabolism in Mammals. *Cell* **175**, 502–513.e13 (2018). doi:10.1016/j.cell.2018.08.040 Medline

45. K. Shibata, T. Nakai, T. Fukuwatari, Simultaneous high-performance liquid chromatography determination of coenzyme A, dephospho-coenzyme A, and acetyl-coenzyme A in normal and pantothenic acid-deficient rats. *Anal. Biochem.* **430**, 151–155 (2012). doi:10.1016/j.ab.2012.08.010 Medline

46. D. Kim, S. L. Salzberg, TopHat-Fusion: An algorithm for discovery of novel fusion transcripts. *Genome Biol.* **12**, R72 (2011). doi:10.1186/gb-2011-12-8-r72 Medline

47. M. D. Robinson, D. J. McCarthy, G. K. Smyth, edgeR: A Bioconductor package for differential expression analysis of digital gene expression data. *Bioinformatics* **26**, 139–140 (2010). doi:10.1093/bioinformatics/btp616 Medline

48. C. Trapnell, A. Roberts, L. Goff, G. Pertea, D. Kim, D. R. Kelley, H. Pimentel, S. L. Salzberg, J. L. Rinn, L. Pachter, Differential gene and transcript expression analysis of RNA-seq experiments with TopHat and Cufflinks. *Nat. Protoc.* **7**, 562–578 (2012). doi:10.1038/nprot.2012.016 Medline